Explainable Machine Learning for Epileptiform Discharge Detection from Electroencephalogram

PH.D. THESIS

KOSUKE FUKUMORI

A thesis submitted in fulfillment of the requirements

for the degree of Doctor of Philosophy

Department of Electronics and Information Engineering

Tokyo University of Agriculture and Technology

October 31, 2022

Abstract

Epilepsy is a neurological disorder that is said to affect 50 million patients worldwide. In some patients, it can lead to developmental disorders such as ASD and ADHD.

Epilepsy that appears in childhood is called childhood epilepsy. Childhood epilepsy is a complex group of seizure disorders associated with neuropsychological disturbances that are thought to have diverse outcomes during development and later in life. In the case of childhood epilepsy, which affects the growing brain, compared to epilepsy developing at other ages, it may lead to neurodevelopmental disorders such as ASD and ADHD. In some cases, no special treatment is necessary, but in most cases, an accurate diagnosis and appropriate treatment, such as antiepileptic drugs, will allow the patient to live a seizure-free life. Therefore, treatment of childhood epilepsy can lead to a reduction in the number of patients with developmental disorders in the future.

In the treatment of epilepsy, electroencephalography (EEG) is necessarily performed to detect abnormal brain regions and specific symptoms. Because of the lack of experts who have highly skilled knowledge for EEG diagnosis, automated technologies are advancing. These technologies support the diagnostic work of epileptologists. To develop these technologies, machine learning-based methods have been used successfully for detecting epileptic spikes, one of the biomarkers, from EEG. However, designing based on empirical knowledge is essential to build machine learning-based detection systems. This thesis proposed some methods that automate these

design sections that require the human factors required for the entire system in two ways: (1) to automate parameters tuning in the EEG preprocessing step while extracting explainable features, and (2) Eliminate candidate detection methods that rely on human knowledge in EEG segment generation.

For the parameters tuning at EEG preprocessing, this study introduces a novel class of neural networks (NNs) that have a bank of linear-phase finite impulse response filters at the first layer as a preprocessor that can behave as bandpass filters that extract biomarkers without destroying waveforms because of a linear-phase condition. Besides, the parameters of the filters are also data-driven. The proposed NNs were trained with a large amount of clinical EEG data, including 15,833 epileptic spike waveforms recorded from 50 patients, and their labels were annotated by specialists. In the experiments, we compared three scenarios for the first layer: no preprocessing, discrete wavelet transform, and the proposed data-driven filters. The experimental results show that the trained data-driven filter bank with supervised learning behaves like multiple bandpass filters. In particular, the trained filter passed a frequency band of approximately 10–30 Hz.

However, in the above method, the EEG segments for input into the detection model were generated based on the label locations annotated by the epileptologists. In other words, the waveforms that are candidates for identification must be previously determined to drive the model. Therefore, it is difficult to detect epileptic EEG from the entire EEG because the above study is a classification task using epileptic and non-epileptic EEG segments. To address this problem, this study hypothesize that a machine learning model could extract locations and ranges of particular interest within a segment to detect epileptic spikes while simplifying the rules for EEG segment creation. With this method, the location of the EEG signal of interest within a segment is not fixed, thus the learning model must identify its location.

In this thesis, to locate the waveforms of interest, we introduces the Satelight model, which uses the self-attention (SA) mechanism. The SA mechanism is expected to reduce the number of parameters and efficiently extract features from a small amount of EEG data. The model was trained using a clinical EEG dataset labeled by five specialists, including 16,008 epileptic spikes and 15,478 artifacts from 50 children. To validate the effectiveness, we compared various spike detection approaches with the clinical EEG data. The experimental results showed that the proposed method detected epileptic spikes more effectively than other models (accuracy $= 0.876$ and false positive rate $= 0.133$). Further exploration of the hidden parameters revealed that the model automatically attended to the EEG's characteristic waveform locations of interest.

The proposed solutions showed that the machine learning-based model automatically learned the expert knowledge by the models themselves. These results could provide significant assistance to epileptologists and increase the number of EEG analyses of patients with intractable epilepsy.

Declaration of Authorship

I, Kosuke FUKUMORI, declare that this thesis titled, "Explainable Machine Learning for Epileptiform Discharge Detection from Electroencephalogram" and the work presented in it are my own. I confirm that:

- This work was done wholly or mainly while in candidature for a research degree at this University.
- Where I have consulted the published work of others, this is always clearly attributed.
- Where I have quoted from the work of others, the source is always given. With the exception of such quotations, this thesis is entirely my own work.
- I have acknowledged all main sources of help.
- Where the thesis is based on work done by myself jointly with others, I have made clear exactly what was done by others and what I have contributed myself.

Signed:

_____

Date:

_____

Acknowledgements

First and foremost I would like to express my appreciation and gratitude to my superviser, Prof. Toshihisa Tanaka. His support and guidance have make the completion of this thesis possible. His guidance with patience and knowledge is the ultimate outcome of this thesis. Without his generous help it would have been impossible to finish this work. I would like to thanks epilepsy specialists, Dr. Noboru Yoshida, Dr. Hidenori Sugano, Dr. Madoka Nakajima, and Dr. Yasushi Iimura. In addition, I would also like to thanks Ms. Meiko Sakurai and Ms. Junko Hirota for their help with dataset collection. I am also grateful to my wife, family, and all of my co-workers including Riken AIP. They have always been supportive and I never forget that. This work was supported by JST CREST Grant Number JPMJCR1784.

Contents

List of Figures

List of Tables

List of Abbreviations

EEG	**E**lectro**E**ncephalo**G**ram
CECTS	**C**hildhood **E**pilepsy with **C**entro**T**emporal **S**pikes
ASD	**A**utism **S**pectrum **D**isorders
ADHD	**A**ttention-**D**deficit **H**hyperactivity **D**disorder
DWT	**D**iscrete **W**avelet **T**ransform
RF	**R**andom **F**orest
ANNs	**A**rtificial **N**eural **N**etworks
CNNs	**C**onvolutional **N**eural **N**etworks
LPCL	**L**inear-**P**hase **C**onvolutional **L**ayer
ROC	**R**eceiver **O**perating **C**haracteristic
AUC	**A**rea **U**nder the **C**urve

Dedicated to all video games...

Chapter 1

Introduction

1.1 Epilepsy

Epilepsy is a chronic brain condition that results in seizures characterized by disorientation and convulsions associated with excessive electrical stimulation of brain neurons [1]. Epilepsy affects about 50 million people worldwide, and there is a severe shortage of specialists who treat epilepsy (epileptologists). For example, Japan only has 700 epileptologists, regardless of having one million patients suffering from epilepsy [2]. One of the symptoms, epileptic seizures, is defined as the occurrence of transient signs and symptoms characterized by sudden and involuntary skeletal muscle activity due to abnormal, excessive, or synchronized neuronal activity in the brain. Early diagnosis and treatment, as well as specific medical support, are necessary to prevent status epilepticus superimposition [3]. Various factors have been considered in the etiology of epilepsy, including structural, genetic, and immunologic factors. However, in most cases, the etiology of patients with epilepsy is unknown. Furthermore, epilepsy can lead to comorbidities such as cognitive, neurodevelopmental, and behavioral disorders. For some patients, these comorbidities have a greater impact than epilepsy and can significantly interfere with daily life [4]. In particular, neurodevelopmental disorders are defined as a group of disorders that develop

during the developmental years and induce impairments that result in functional disability. Neurodevelopmental disorders include autism spectrum disorders (ASD), attention-deficit hyperactivity disorder (ADHD), and intellectual disabilities [5].

1.2 Childhood Epilepsy

Epilepsy that appears in childhood is called childhood epilepsy. Childhood epilepsy is a complex group of seizure disorders associated with neuropsychological disturbances that are thought to have diverse outcomes during development and later in life. A study in Italy reported that the peak incidence of epilepsy is in children under 15 years of age (newly 50.14 patients per 100,000 children per year) [6].

In the case of childhood epilepsy, which affects the growing brain, compared to epilepsy developing at other ages, it may lead to neurodevelopmental disorders such as ASD and ADHD [7]. In addition, ADHD has a prevalence of 7–9% in the general pediatric population. On the other hand, in children with epilepsy, ADHD has been found to be present in 20% to 50% of patients [8]. In some cases, no special treatment is necessary, but in most cases, an accurate diagnosis and appropriate treatment, such as antiepileptic drugs, will allow the patient to live a seizure-free life. Therefore, treatment of childhood epilepsy can lead to a reduction in the number of patients with developmental disorders in the future.

1.3 Types of Childhood Epilepsies

Childhood epilepsy is not a single case, but rather a generic term for a variety of cases. Detailed epilepsy cases are defined by the type of seizures experienced, age of onset, neurological status, and physical examination. The reason for classifying epilepsy in this manner is to facilitate understanding of possible treatments and specific prognoses [9]. The following epilepsy types are specific examples.

1.3.1 Infantile Spasms and West Syndrome

West syndrome is characterized by epileptic convulsions. This case was first reported in 1841 [10]. These epileptic seizures are characterized by various muscle contractions, including head nodding and body flexion, and occur in clusters. The EEG during interictal has a high-voltage, acyclic, and highly abnormal pattern [11].

1.3.2 Benign Partial Epilepsies of Childhood

Benign partial epilepsy of childhood is a group of disorders that are considered to be genetically transmitted and are often associated with characteristic EEG patterns [11]. One of the more specific cases, benign epilepsy with centrotemporal spikes (BECTS), is the most common focal epilepsy syndrome in children, accounting for 15–20% of all childhood epilepsies. BECTS is also known as childhood epilepsy with centro-temporal spikes (CECTS) [12] The typical age of onset is 5 to 8 years. Seizures are relatively rare overall, with 60–70% of patients experiencing 2–10 seizures during their lifetime and 10–20% experiencing only one seizure. Symptoms of epilepsy may be activated by sleep. The characteristic EEG change, as suggested by

its name, is a steady spike followed by a slow wave that occurs either unilaterally or bilaterally [13].

1.3.3 Childhood Absence Epilepsy

Pediatric absence epilepsy (CAE) accounts for approximately 8% of pediatric epilepsy cases [14]. The main symptom of CAE is absence seizures, which are characterized by brief staring, subtle rhythmic blinking of the eyes, and unawareness of surroundings [9]. It has been reported to cause learning disabilities and cognitive impairment in the future. In addition, young adults with a history of CAE have a high rate of work and social difficulties, persistent difficulties with family and friends, less regular outings with friends and partners, and mental and emotional difficulties [14].

1.4 Epilepsy Diagnosis

For the diagnosis of epilepsy, a variety of methods are used, including magnetic resonance imaging (MRI), computed tomography (CT), positron emission tomography (PET), magnetoencephalography (MEG), and electroencephalography (EEG) [15]. Among these methods, EEG diagnostics are particularly important in identifying epileptic EEG and brain regions of interest by measuring temporal and spatial information of the brain as voltage [16, 15]. One of the main purposes of EEG diagnostics is the observation of waveforms that appear during interictal seizures, called epileptic spikes. These spikes are caused by synchronous firing of high neuronal populations and are considered an unusual phenomenon [17]. Furthermore, the location and frequency of these spikes can be helpful as a biomarker for diagnosing epilepsy type. However, accurate diagnosis and identification of epileptic

types usually requires monitoring the patient's EEG for several days. This manual EEG monitoring is very time-consuming [18].

1.5 Studies of Automated Epileptic Spike Detection

1.5.1 Preprocessing methods for EEG

To support the detection of epileptic spikes, several automated detection approaches are making great advances [19, 20, 21, 22, 23, 24, 25, 26]. To implement the automatic detection of epileptic spikes, supervised learning is one effective method. To efficiently train the machine learning models, the EEG signal is generally decomposed into standard clinical frequency bands of interest—such as δ, θ, α, β, and γ—before the learning [27]. While conducting such training, it is necessary to select the frequency bands appropriately, which depends on several factors, such as the EEG measurement method, measurement environment, the type of epilepsy, and epileptologists' skills. However, in various studies, a range of frequencies or frequency bands of interest has been empirically selected.

Cheong et al. [28] used discrete wavelet transform (DWT) to decompose the signal into frequency subbands from the delta band to the gamma band (0–63 Hz). Gutierrez et al. [20] applied a bandpass filter in the range of 0.5–70 Hz. Then, they obtained wavelet coefficients from the filtered signal to classify epileptic spikes. Similarly, a range of 0.5–70 Hz was extracted with a Butterworth filter to obtain wavelet coefficients [26].

Other studies have utilized narrow bandpass filter ranges for preprocessing. Polat et al. [29] applied a bandpass filter range of 0.53–40 Hz and

then used the discrete Fourier transform to extract the features for the decision tree classifier. Khan et al. [23] used the range of 0–32 Hz decomposed by DWT because most of epileptic information lies in the range of 0.5–30 Hz. Similarly, Douget et al. [19] and Indiradevi et al. [30] adopted DWT with Daubechies 4 (DB4) to extract the frequency band of 4–32 Hz. Moreover, Fergus et al. [31] used the range of only 0–25 Hz, although they did not use DWT but a Butterworth filter. Thereafter, they employed the holdout technique and k-fold cross-validation, passing into many different classifier models for distinguishing seizure and nonseizure EEG records.

In these studies for the classification or detection of epilepsy, DWT decomposition and other filtering methods were effective. As seen above, although the frequency range, including the epileptic information, is roughly known to be less than about 60 Hz, the selection of cut-off frequencies depends on several factors, such as the designer of the automated system, the type of epilepsy, the epileptologists on diagnosis, and so forth. This motivated us to identify the filter parameters based on data.

1.5.2 Neural Network-Based Techniques

Neural network (NN)-based techniques have demonstrated high performance in spike detection tasks [32, 33, 19, 34, 35]. Epileptic spikes have been detected on a single-electrode EEG. Although the shape of the epileptic waveforms is similar among patients, each patient's distribution of the waveforms is unique. To identify these individual differences in distribution among patients, specialists use several montages in epilepsy diagnosis, like bipolar and monopolar, to observe EEGs. This is because the specialists use the EEG of the surrounding or all electrodes to identify epileptic spikes. Therefore, to effectively use the detection methods from a single-electrode EEG, the appropriate montage must be determined manually, limiting its

versatility. These facts have influenced studies on machine learning-based automatic spike detection. Since 2019, numerous related studies have used multi-electrode EEG to detect the location of epileptic spikes[36, 37, 26, 38, 39].

For detecting spikes using these multi-electrode EEG, convolutional NN (CNN)-based models, such as the model by Thomas et al.'s [38] and SpikeNet [37], are some of the effective methods. Thomas et al. [38] used CNN to detect epileptic spikes from multi-electrode EEG by calculating the probability of the appearance of epileptic spikes for individual electrodes and then obtaining the maximum of the output probabilities for all electrodes. SpikeNet [37] directly outputs a predicted value from a multi-electrode EEG segment. This was achieved using a combination of deep convolution layers in the spatial and temporal directions. SpikeNet efficiently extracts features using a top convolutional layer that merges the relationships between electrodes and 22 temporal convolutional layers. According to Thomas et al. [37], SpikeNet outperforms the detection performance of the commercially available software, Persyst13 [40], in spike detection.

1.6 Our Contributions

1.6.1 Extraction of frequency bands of interest for spike detection

Frequency filtering to EEG with the appropriate passbands is essential for enhancing the epileptic spikes. However, in various studies, a range of frequencies or frequency bands of interest has been empirically selected [19, 20, 21, 22, 23, 24, 25, 26]. To solve this limitation, we introduces a novel class

of neural networks (NNs) that have a bank of linear-phase finite impulse response filters at the first layer as a preprocessor that can behave as bandpass filters that extract biomarkers without destroying waveforms because of a linear-phase condition. Besides, the parameters of the filters are also data-driven. The proposed NNs were trained with a large amount of clinical EEG data, including 15,833 epileptic spike waveforms recorded from 15,004 patients, and their labels were annotated by specialists. In the experiments, we compared three scenarios for the first layer: no preprocessing, discrete wavelet transform, and the proposed data-driven filters. The experimental results show that the trained data-driven filter bank with supervised learning behaves like multiple bandpass filters. In particular, the trained filter passed a frequency band of approximately 10–30 Hz.

1.6.2 Identification of temporal location for spike detection

Deep convolutional neural network-based models have been used successfully for detecting epileptic spikes, one of the biomarkers, from EEG [37, 38]. However, a sizeable number of supervised EEG records are required for training [41]. To solve this problem, This study introduces the Satelight model, which uses the self-attention (SA) mechanism. The model was trained using a clinical EEG dataset labeled by five specialists, including 16,008 epileptic spikes and 15,478 artifacts from 50 children. The SA mechanism is expected to reduce the number of parameters and efficiently extract features from a small amount of EEG data. To validate the effectiveness, we compared various spike detection approaches with the clinical EEG data. The experimental results showed that the proposed method detected epileptic spikes more effectively than other models (accuracy $= 0.876$ and false positive rate $= 0.133$). The proposed model had only one-tenth the number of parameters as the other effective model, despite having such a

high detection performance. Further exploration of the hidden parameters revealed that the model automatically attended to the EEG's characteristic waveform locations of interest.

1.7 Organization of Thesis

As shown in Figure 1.1, this thesis is divided into five chapters. Chapter 1 describes the research background, problems, and proposed methodology. Chapter 2 presents the basic machine learning techniques for EEG. Chapter 3 proposes a frequency identification method for spike detection. Chapter 4 proposes a lightweight machine learning model for identifying temporal spike locations. Finally, Chapter 5 summarizes this thesis.

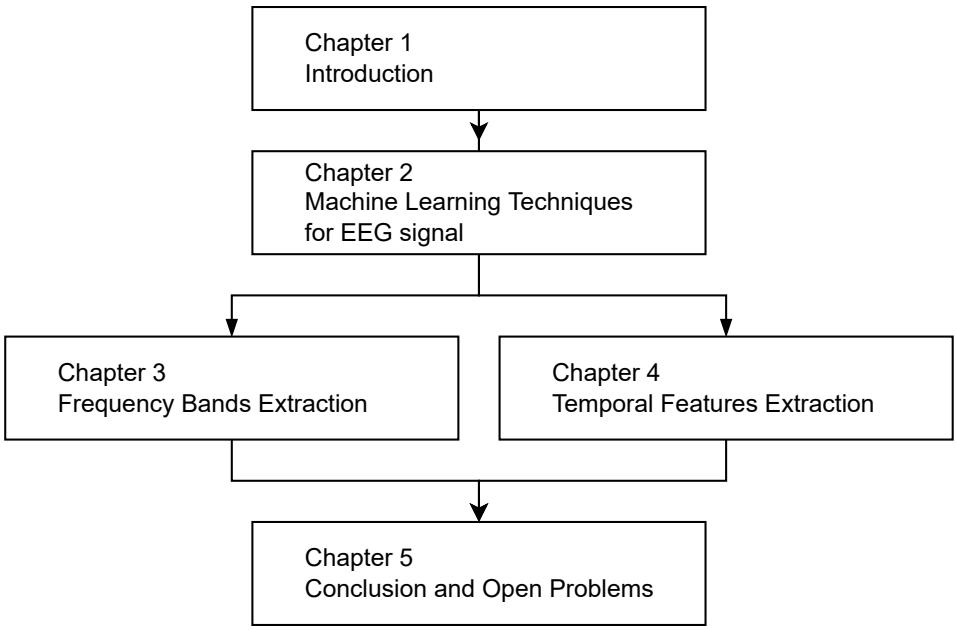

FIGURE 1.1: Diagram for the organization of the thesis.

Chapter 2

Machine Learning Techniques for EEG signal

In this chapter, we introduce some machine learning-based methods, which can be used to the real world signals.

2.1 Convolutional Neural Networks

A type of neural network (NN) that demonstrates excellent performance—especially in the field of image or video recognition [42, 43]—is the CNN. The CNN is an extended NN that has an input layer, multiple hidden layers, and output layer. In general, the hidden layers consist of convolutional layers, and a fully connected layer is used as the output layer. The convolution layer applies a convolution to the input and forwards the result to the next layer. Let $X = \{x_0, x_1, \ldots, x_{N-1}\}$, $Y = \{y_0, y_1, \ldots, y_{M-1}\}$, and $H = \{h_0, h_1, \ldots, h_{L-1}\}$ be a 1D input signal, a 1D output signal, and a convolutional kernel, where N, M, and L are the length of X, Y, and H, respectively. For the sake of simplicity, L is assumed to be even. Focusing on one layer, the input X is convolved with the kernel H, and the output Y is

generated as follows:

$$y_m = \sum_{l=0}^{L-1} h_l x_{m+l}. \tag{2.1}$$

The flattened layer smoothes multiple convolved signals into a single dimension. Then, the fully connected layer multiplies all input neurons by their weight coefficients and connects them to the output.

Some recent studies have applied a CNN-based model to EEG signals [44, 35, 32, 45]. Ullah et al. [44] used 1D convolution to extract features by filtering time series EEG. Zhou et al. [45] directly input both of the multichannel time series EEG signals and their frequency domain signals into a CNN-based model. Such studies using CNN to detect epileptic seizures or epileptic spikes have been gaining interest.

2.2 Separable Convolution

A layer known as separable convolution, which independently convolves the temporal and spatial directions, should be inserted at the beginning of the network for the analysis of multi-electrode EEG with NNs. This involves frequency filtering for the temporal convolution and electrode coupling for the spatial convolution (i.e., montage optimization). Given that it has a separate kernel for each dimension, this convolutional layer has much smaller parameters than a standard two-dimensional convolutional layer. The first model to use this layer for EEG analysis is EEGNet [46], which has been successful in the field of brain-computer interface. Huang et al. [47] also reported the effectiveness of the EEGNet-based model in their study of EEG-based emotion classification tasks . Using an extended model of EEGNet, Shoji et al. [48] successfully identified abnormal EEG durations indicative

of patients with juvenile absence epilepsy. Furthermore, SpikeNet [37] uses a separable convolution to detect epileptic spikes. As these results show, the separable convolution in multi-electrode EEG analysis is effective, particularly in extracting features along the electrode direction.

2.3 Self-Attention Mechanism

Accurately detect epileptic spikes, even in randomly extracted EEG segments, without using candidate detectors. However, to train a deep learning model with many parameters [41], a significant amount of training data are needed. We focused on the SA mechanism to efficiently analyze the waveform of interest. The SA mechanism is expected to automatically skip redundant data in time-series signals [49]. Using the dot-product attention [50] is one way to construct SA. That is, the layer based on SA calculates three hidden features, $\boldsymbol{Q}^{(i)} \in \mathbb{R}^{\tau \times d}$, $\boldsymbol{K}^{(i)} \in \mathbb{R}^{\tau \times d}$, and $\boldsymbol{V}^{(i)} \in \mathbb{R}^{\tau \times d}$, from the input features $\boldsymbol{X}^{(i)} \in \mathbb{R}^{\tau \times d}$ using the three weight matrices, $\boldsymbol{W}_Q \in \mathbb{R}^{d \times d}$, $\boldsymbol{W}_K \in \mathbb{R}^{d \times d}$, and $\boldsymbol{W}_V \in \mathbb{R}^{d \times d}$, as follows:

$$\boldsymbol{Q}^{(i)} = \boldsymbol{X}^{(i)} \boldsymbol{W}_Q, \tag{2.2}$$

$$\boldsymbol{K}^{(i)} = \boldsymbol{X}^{(i)} \boldsymbol{W}_K, \tag{2.3}$$

$$\boldsymbol{V}^{(i)} = \boldsymbol{X}^{(i)} \boldsymbol{W}_V, \tag{2.4}$$

where i, τ, and d are the index of EEG segments, the temporal length of the input feature, and the number of feature electrodes, respectively. Then, using the softmax function and one weight matrix $\boldsymbol{W}_O \in \mathbb{R}^{d \times d}$, the output of the SA layer $\boldsymbol{Y}^{(i)} \in \mathbb{R}^{\tau \times d}$ is obtained as follows:

$$\boldsymbol{Y}^{(i)} = \mathrm{softmax}\left(\boldsymbol{Q}^{(i)} (\boldsymbol{K}^{(i)})^{\top}\right) \boldsymbol{V}^{(i)} \boldsymbol{W}_O. \tag{2.5}$$

As (2.5) shows, the softmax function of the matrix product between $\boldsymbol{Q}^{(i)}$ and $\boldsymbol{K}^{(i)}$ acts to represent the level of interest within the input feature itself. Further, it is expected that multiplying the softmax using the weighted input feature $\boldsymbol{V}^{(i)}$ extracts meaningful EEG locations for the prediction. Here, the SA layer can be constructed as a single layer using these calculations.

Chapter 3

Frequency Bands Extraction

In this chapter, we introduce a novel class of NNs that have a bank of linear-phase finite impulse response filters at the first layer as a preprocessor that can behave as bandpass filters that extract biomarkers without destroying waveforms because of a linear-phase condition. Besides, the parameters of the filters are also data-driven. The proposed NNs were trained with a large amount of clinical EEG data, including 15,833 epileptic spike waveforms recorded from 50 patients, and their labels were annotated by specialists. In the experiments, we compared three scenarios for the first layer: no preprocessing, discrete wavelet transform, and the proposed data-driven filters. The experimental results show that the trained data-driven filter bank with supervised learning behaves like multiple bandpass filters.

3.1 Proposed method

3.1.1 Dataset Construction

EEG recordings were collected from 50 patients (24 males and 26 females) with childhood epilepsy with centro-temporal spikes (CECTS) [12] at the Department of Pediatrics, Juntendo University Nerima Hospital. The age range of the patients at the time of the examination was 3–12 years. The data were recorded from 16 electrodes with the international 10–20 methods

using the Nihon Koden EEG-1200 system. The sampling frequency was 500 Hz. This dataset was recorded and analyzed with the approval of the Juntendo University Hospital Ethics Committee and the Tokyo University of Agriculture and Technology Ethics Committee.

First, two neurosurgeons, one pediatrician, and one clinical technologists selected a focal channel associated with the origin of the epileptic spike. In particular, CECTS is a type of focal epilepsy in which spikes appear only in a certain channel. Therefore, the annotators chose the most epileptic intense channel as the annotation channel. Peaks (minima and maxima) of the EEG at the channel were detected by a peak search function implemented with Scipy [51]. This function extracts both upward and downward peaks with a minimum distance of 100 points. Using a threshold determined at the 80th percentile value in the absolute amplitude of all peaks, meaningless peaks caused by noise, and so forth were removed. Second, the annotators labeled each peak as either an epileptic spike (spike or spike-and-wave) or nonepileptic discharge. These non-epileptic waveforms were carefully selected by the annotator from noise peaks excluding extreme voltage fluctuations caused by body movements and sweating and other possible interferences. Then, a 1-s segment was extracted at every detected peak, including 300 ms before and 700 ms after the peak. Fig. 3.1 illustrates an example of typical waveforms. Z-score normalization was applied with the mean value and standard deviation for each segment. It should be noted that each segment represents one candidate spike.

3.1.2 Preprocessing and Subband Decomposition

We considered two models, as shown in Fig. 3.2. The first model uses a predefined bank of filters. It is based on the method adopted in several previous studies. The second model involves a special convolution layer

called the *linear-phase convolutional layer* (LPCL) in which the parameters are searched based on the dataset.

Fixed approach

The first approach employs a hand-engineered preprocessing technique for each segment. DWT is applied to extract the subbands from the EEG. In this paper, the Daubechies wavelet of order 4 (DB4), which has been reported to be appropriate for analyzing EEG signals [19, 52, 53], is adopted as the mother wavelet. The input EEG is decomposed into six coefficient levels—D6, D5, D4, D3, D2, and D1—and one approximation level, A6. Then, four subbands corresponding to D6, D5, D4, or D3 are generated. Each subband represents the θ band (4–8 Hz), the α band (8–16 Hz), the β band (16–32 Hz), and the γ band (32–64 Hz), respectively [28]. The approximation level, A6, and the coefficient levels, D2 and D1, are eliminated because the low-frequency band may include breathing and eye movements. The high-frequency band can be considered noise.

Novel data-driven approach using linear-phase convolutional layer

The convolutional layer described in Section 2.1 can behave as a finite impulse response (FIR) filter. However, each weight in a convolutional layer is fitted with a high degree of freedom, although FIR filters are designed with a linear-phase (LP) constraint to preserve the waveform shape. This paper proposes a convolutional layer with LP constraints, that is, the LPCL, and its implementation.

The FIR filter is realized by convolution of the discrete signal $X = \{x_0, x_1, \ldots, x_{N-1}\}$ and the kernel $H = \{h_0, h_1, \ldots, h_{L-1}\}$, and the output discrete signal $Y = \{y_0, y_1, \ldots, y_{M-1}\}$ is calculated based on the current and past $L - 1$ inputs,

much like (2.1). Generally, the kernel described above causes phase distortion, which can be avoided by imposing an LP constraint. When the length of the filter is even, the even symmetry and odd symmetry of the kernel yields the LP FIR filter of type-Ⅱ and type-Ⅳ [54], that is:

$$h_l = h_{L-1-l}, \tag{3.1}$$

and

$$h_l = -h_{L-1-l}, \tag{3.2}$$

respectively. The idea behind using type-Ⅱ and type-Ⅳ symmetric filters is twofold: (a) In generalizing the Haar transform to a bank of FIR filters, the multistage Haar wavelet transform is equivalent to an orthogonal matrix [55], including type-Ⅱ and type-Ⅳ FIR filters with different lengths, and each filter corresponds to a bandpass filter. (b) By using type-Ⅱ and type-Ⅳ, it is possible to compose a bank of lowpass, bandpass, and highpass filters because type-Ⅱ and type-Ⅳ are inherently unable to yield a highpass filter and a lowpass filter, respectively [54].

From (2.1) and (3.1), an even symmetric convolution $Y^e = \{y_0^e, y_1^e, \ldots, y_M^e\}$ is described as follows:

$$y_m^e = \sum_{l=0}^{L/2-1} h_l \left(x_{m+l} + x_{m+(L-1)-l} \right). \tag{3.3}$$

This convolution can be implemented using a lattice structure [56], as shown in Fig. 3.3(a). As shown in this figure, even symmetric convolution can be regarded as the product of the vector expressed by the addition of the two components in X and kernel H. This is the same operation as a weighted full connection (namely, a fully connected layer). Therefore, this can be implemented by repurposing a conventional neural network framework with

the addition of X elements, as illustrated in Fig. 3.3(a). Similarly, an odd symmetric convolution $Y^o = \{y_0^o, y_1^o, \ldots, y_M^o\}$ is described as follows:

$$y_m^o = \sum_{l=0}^{L/2-1} h_l \left(x_{m+l} - x_{m+(L-1)-l} \right). \tag{3.4}$$

Fig. 3.3(b) illustrates the lattice structure for (3.4). As this figure shows, the odd symmetric convolution can be implemented by repurposing a conventional neural network framework with the subtraction of X elements. These LPCLs can replace the fixed (predesigned) subband filters, as illustrated in Fig. 3.2. The idea is hypothesized that the LPCL can derive the frequency bands of interest from the epileptic EEG dataset.

3.1.3 Classifier Models

Random forest (RF), ANN, and CNN are adopted as the classifiers. Although the ANN and CNN can be combined with either a traditional preprocessing technique or the proposed method, RF can be combined only with the traditional preprocessing technique.

The RF parameters are tuned using a grid search for the parameters listed in Table 3.1. To adjust the grid search, the F1 score is used as the ranking score, and fivefold cross-validation with two subsets is used. The model architectures of the ANN and CNN are depicted in Fig. 3.4. To generate the initial weights of these models, the He initializer [57] is used for the layers that employ the rectified linear unit (ReLU) as the activation function. The Xavier initializer [58] is used for the other layers. These neural networks are fitted by the Adam optimizer [59] (the learning rate η and the scale parameters β_1 and β_2 are 0.001, 0.9, and 0.999, respectively) with batch size 256 while suppressing overfitting using early stopping [60].

3.1.4 Application of the Linear-Phase Convolutional Layer

In this paper, eight LPCLs are connected in parallel to the classification model, as illustrated in Fig. 3.2(b). Each LPCL setting is as shown in Table 3.2. As in this table, there are LPCLs with different filter lengths to let the model select filters that contribute to the classification. These kernel lengths are set based on the length of the Haar transform matrix induced from the Haar wavelet [55]. That is, filter lengths of 8, 16, 32, and 64 are expected to extract the standard clinical bands of γ, β, α, and θ, respectively. At the LPCL's filtering, the stride length is 1, and the input signal is padded with zero to keep the input and output lengths invariant. For the initialization of the coefficients in these LPCLs, the Xavier initializer [58] is used.

3.1.5 Evaluation

To validate the effectiveness of the proposed method, an experiment is performed using the dataset described in Section 3.1.1. Recall that the classification is binary: an epileptic spike or a nonepileptic discharge. For comparison, three approaches are used: the fixed approach, the proposed data-driven approach, and an approach without preprocessing. Combining these approaches with the three classification models, a total of eight methods are compared, as shown in Table 3.3. In the fixed approach, a 1-s raw EEG is decomposed into four frequency bands (θ, α, β, and γ bands) using DWT. In the proposed approach, because the LPCLs act as a bank of FIR filters, a 1-s segment is input to this layer. Furthermore, in the third approach, a

TABLE 3.1: Parameter for the random forest to be tuned by grid search

Parameter	Candidates
Number of trees N_{tree}	5, 10, 20, 30, 50, 100, 300
Maximum depth $D_{\max}$	2, 4, 6, 8, 10

1-s segment is input directly into the classification model. This approach is similar to our previous work [35].

In the experiment, intersubject validation in all combinations is performed, in which 49 patients are used as training data and the remaining patient is used for the test data. To evaluate the models, the area under the curve (AUC), F1 value, sensitivity, and specificity are employed. AUC is the area of the curve drawn by the false positive rate (FPR) and the true positive rate (TPR = Sensitivity) when the discrimination threshold is changed, and it is calculated in the following manner:

$$\mathrm{FPR} = \frac{\mathrm{FP}}{\mathrm{FP} + \mathrm{TN}}, \tag{3.5}$$

$$\mathrm{TPR} = \frac{\mathrm{TP}}{\mathrm{TP} + \mathrm{FN}} \tag{3.6}$$

$$= \mathrm{Sensitivity}, \tag{3.7}$$

where TP, FP, FN, and TN are the numbers of a true positive, false positive, false negative, and true negative, respectively. The specificity is the true negative rate, which is calculated as follows:

$$\mathrm{Specificity} = \frac{\mathrm{TN}}{\mathrm{TN} + \mathrm{FP}}. \tag{3.8}$$

The F1 value is calculated as the harmonic mean of the precision and sensitivity. These metrics are defined as follows [61]:

$$\mathrm{Precision} = \frac{\mathrm{TP}}{\mathrm{TP} + \mathrm{FP}}, \tag{3.9}$$

$$\mathrm{F1} = \frac{2 \cdot \mathrm{Precision} \cdot \mathrm{Sensitivity}}{\mathrm{Precision} + \mathrm{Sensitivity}}. \tag{3.10}$$

In particular, this paper employs the mean AUC and the mean F1 value (by

taking 30 independent realizations) in evaluating the ANN, CNN, and LP-CLs because the initial weight and initial kernel value affect the learning. In addition, because the convolution filter can be regarded as an FIR filter, the frequency response of each filter of the eight LPCLs is analyzed after training. Similar to evaluating the AUC and F1 values, the frequency response is meaned by 30 independent runs.

All experimental results are computed on a high-performance computer built with an AMD(R) EPYC(TM) 7742 CPU@2.25 GHz, 512 GB RAM, and four NVIDIA(R) A100 GPUs. The models in the experiment are constructed using Python 3.7.6 with Keras [62] and Scikit-learn [63].

3.2 Experimental Results

Table 3.4 represents the AUC, F1 value, sensitivity, and specificity by each model and preprocessing technique. This table shows the mean values of all intersubject validations. A statistical tests including Friedman's one-way analysis of variance (ANOVA) [64] showed that the effects of the methods on the four metrics were significant ($F_{\mathrm{AUC}}(1,7) = 294$, $p_{\mathrm{AUC}} = 7.21 \times 10^{-59}$, $F_{\mathrm{F1}}(1,7) = 197$, $p_{\mathrm{F1}} = 2.41 \times 10^{-38}$, $F_{\mathrm{sen}}(1,7) = 205$, $p_{\mathrm{sen}} = 5.89 \times 10^{-40}$, $F_{\mathrm{spe}}(1,7) = 120$, and $p_{\mathrm{spe}} = 3.10 \times 10^{-22}$). Because the main effect of the models has been observed, a Bonferroni *post-hoc* test [64] was performed

TABLE 3.2: Settings of the LPCLs

LPCL no.	Filter length	Constraint type
1	8	even symmetric
2	16	
3	32	
4	64	
5	8	odd symmetric
6	16	
7	32	
8	64	

to better understand the changes in cross-correlation across the different preprocessors. Fig. 4.3 visualizes the numerical results and their analysis of variance of 50 intersubject validations. As shown in Fig. 3.5, significant differences in the AUC results were observed when using the preprocessors, especially for RF and ANN. Moreover, significant differences in the F1 results were observed for all classification models when using the preprocessors. In particular, the F1 results using LPCLs tended to be statistically higher than DWT in the ANN-based comparison. This is because LPCLs statistically increased specificity, as shown in Fig. 3.8. From these results, it can be seen that the preprocessing of EEG affects the classification performance, even with manually designed filters such as DWT. Furthermore, the optimal preprocessing could be learned in a data-driven method with LPCLs.

Fig. 3.9 provides an example of prediction by CNN combined with the LPCL. In this figure, a relatively sharp waveform indicates an epileptic spike, regardless of its amplitude. Figs. 3.10 and 3.11 illustrate examples of the frequency responses at the proposed layers. In addition, Figs. 3.10 and 3.11 show clearly that the proposed method's filter emphasizes the low-frequency band (around 12 Hz). Thus, while the conventional method manually focuses on the low-frequency band, it can be said that the proposed method automatically extracts this frequency. Moreover, Figs. 3.10(b) and

TABLE 3.3: Methods of experimental comparison. The proposed data-driven method is combined only with the neural network models.

Preprocessing	None	DWT	LPCL
Input feature to the following models [#length, #band]	Raw EEG [500, 1]	Decomposed four frequency bands [500, 4]	Learnable eight frequency bands [500, 8]
Combine with RF	✓	✓	
Combine with ANN	✓	✓	✓
Combine with CNN	✓	✓	✓

3.11(b) show that filters with odd symmetric constraints pass different frequency bands according to the filter length.

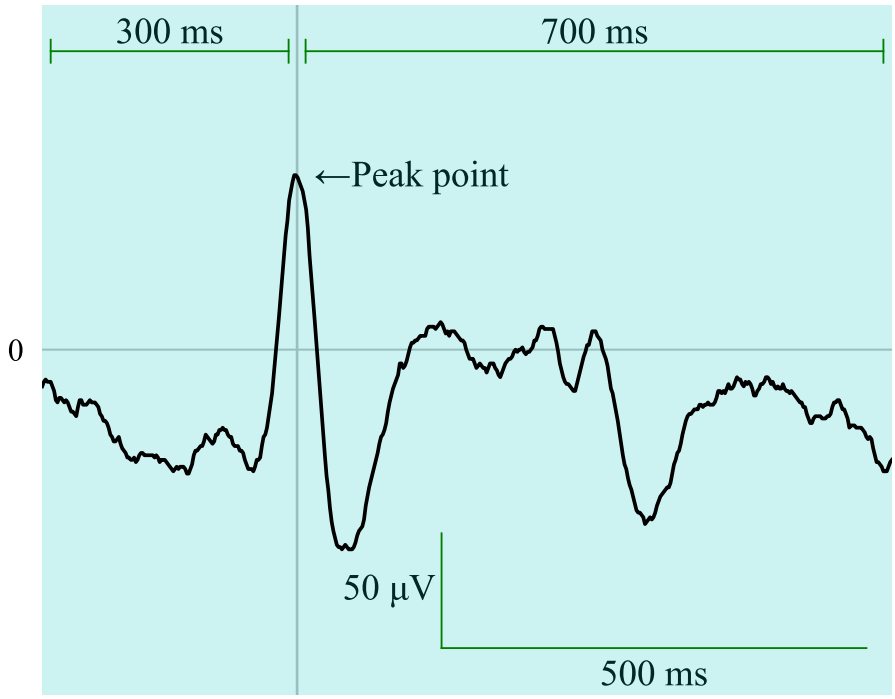

(a) An epileptic spike

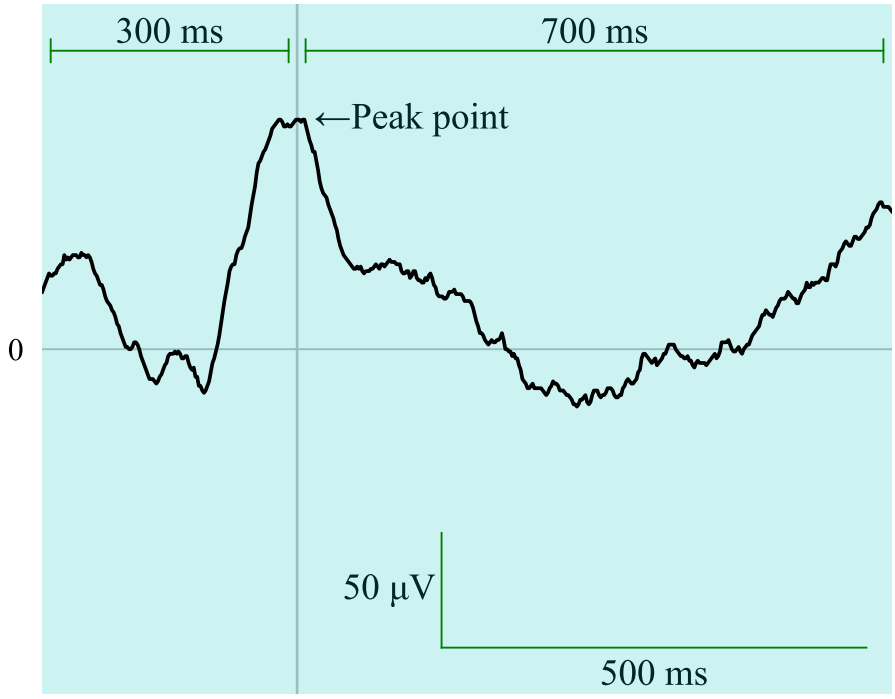

(b) A nonepileptic discharge

FIGURE 3.1: Typical waveforms of detected peaks. Each waveform is clipped into a 1-s segment.

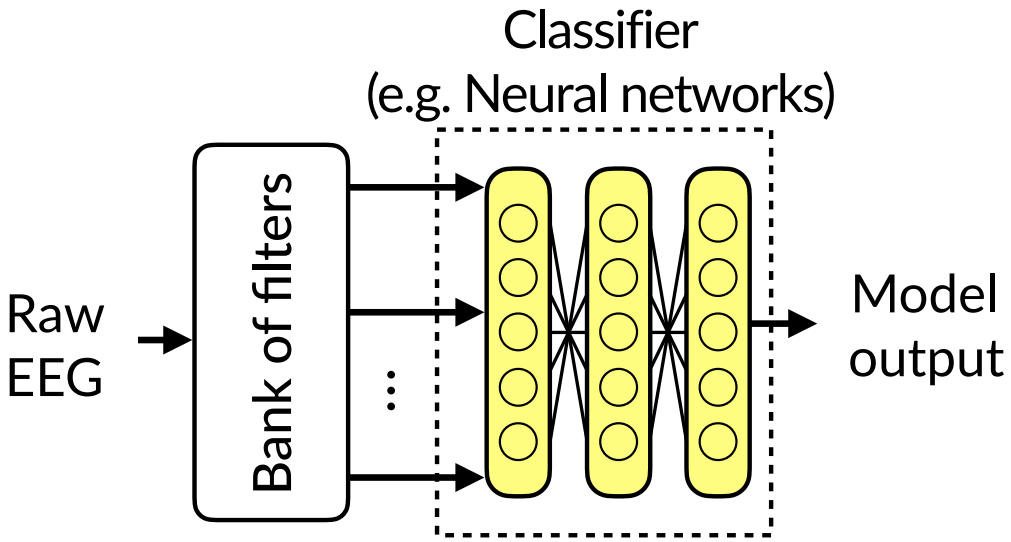

(a) The traditional fixed approach.

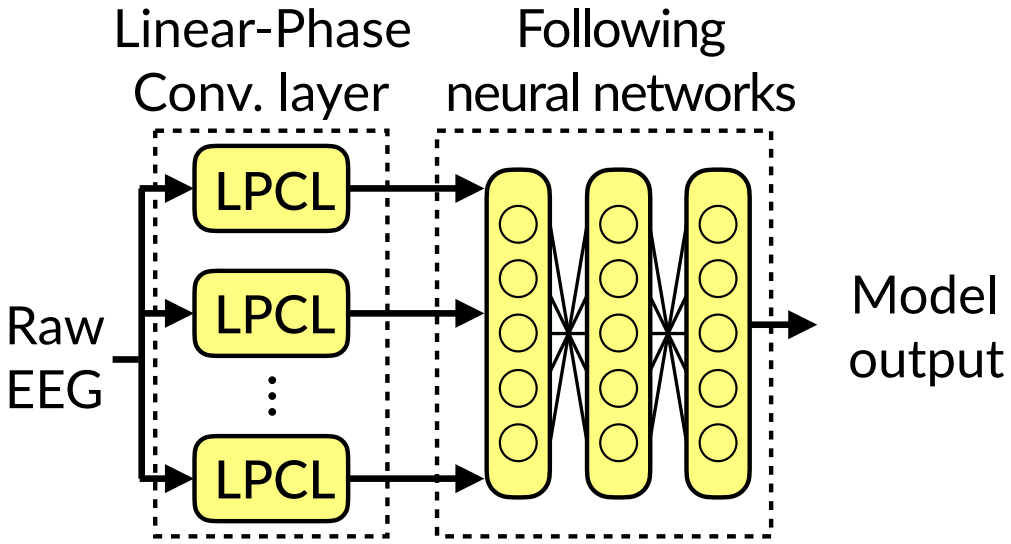

(b) The data-driven approach using the linear-phase convolutional layers.

FIGURE 3.2: Diagrams of the two prediction models. The colored blocks contain parameters to be trained.

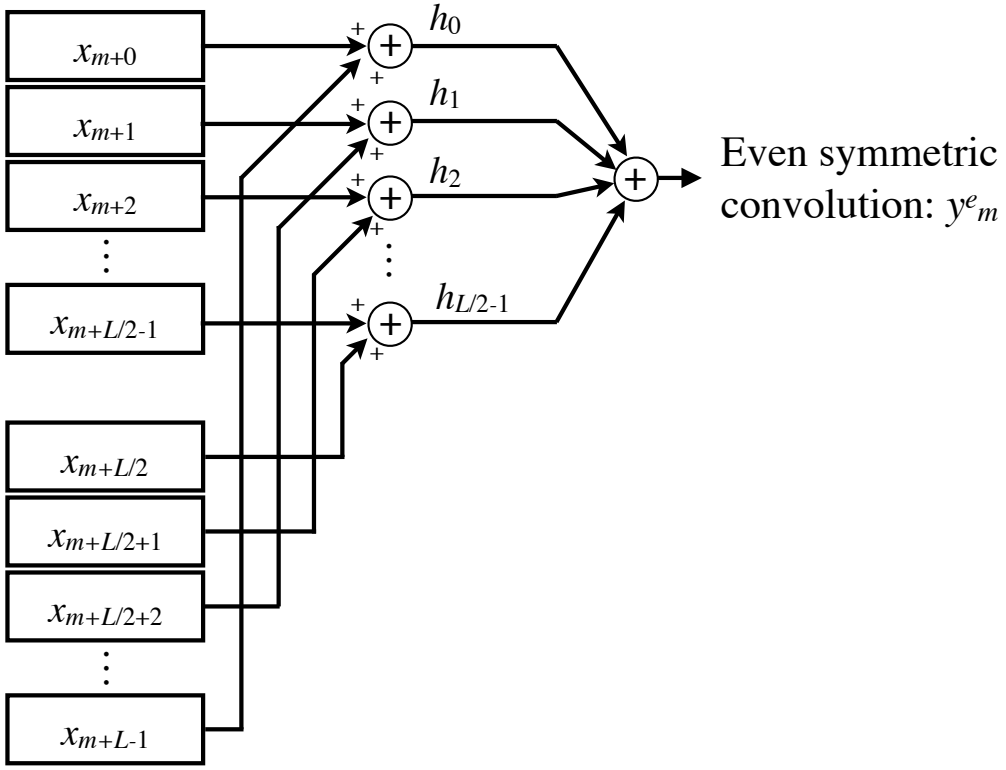

(a) Even symmetric convolution.

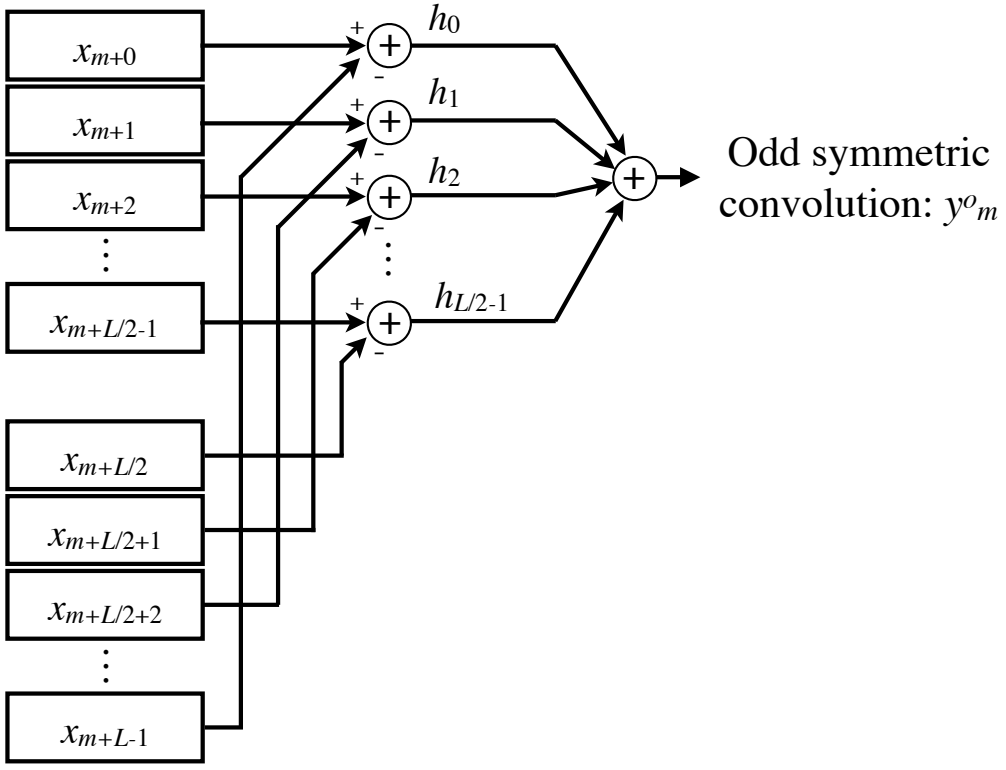

(b) Odd symmetric convolution.

FIGURE 3.3: Lattice structures of the LP convolution.

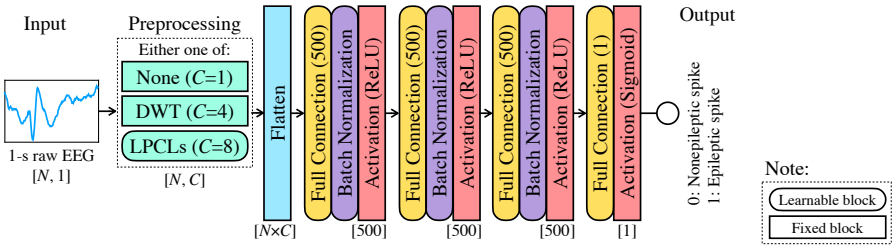

(a) Classification model based on ANN

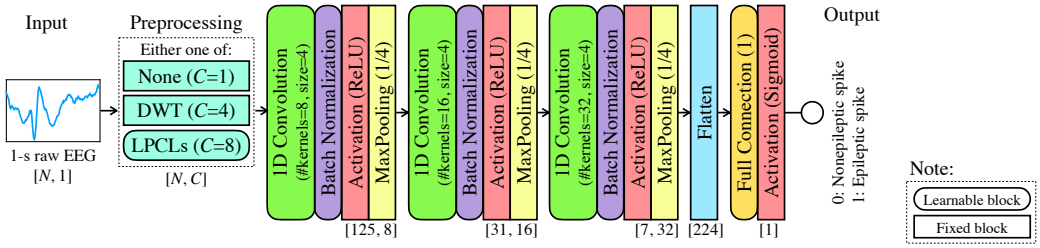

(b) Classification model based on CNN

FIGURE 3.4: The model architectures, where N and C are the length of the input segment and the number of input sub-bands to the following model, respectively. When "None" is selected as the preprocessing, the raw EEG is output without any changes ($C = 1$); when "DWT," four clinical frequency bands are extracted ($C = 4$); when "LPCLs," the raw EEG is preprocessed by the eight LPCLs in Table 3.2 ($C = 8$). Then, the three-stacked ANN and CNN output a prediction value in the range of 0 to 1.

TABLE 3.4: Numerical evaluation results. Total of 50 intersubject validations are conducted, with 30 independent runs per test patient data. Thus, a mean of 1,500 runs is calculated (Mean ± STD). The highest values for each metric are bolded.

Metric	**Classification model**							
	Random forest		ANN			CNN		
	Preprocessor							
	None	DWT	None	DWT	LPCLs	None	DWT	LPCLs
AUC	0.912 ± 7.13E-02	0.941 ± 7.14E-02	0.915 ± 6.76E-02	0.937 ± 5.70E-02	0.944 ± 4.99E-02	0.965 ± 3.80E-02	0.965 ± 3.96E-02	**0.967 ± 3.54E-02**
F1	0.780 ± 1.66E-01	0.838 ± 1.62E-01	0.811 ± 1.68E-01	0.843 ± 1.57E-01	0.850 ± 1.54E-01	0.813 ± 1.79E-01	0.862 ± 1.63E-01	**0.880 ± 1.34E-01**
Sensitivity	0.744 ± 1.96E-01	0.823 ± 1.82E-01	0.827 ± 1.42E-01	0.853 ± 1.38E-01	0.859 ± 1.30E-01	0.773 ± 2.22E-01	0.858 ± 1.74E-01	**0.883 ± 1.31E-01**
Specificity	0.905 ± 6.18E-02	0.915 ± 7.02E-02	0.853 ± 7.52E-02	0.886 ± 7.01E-02	0.904 ± 7.28E-02	**0.944 ± 8.64E-02**	0.931 ± 8.06E-02	0.927 ± 8.01E-02

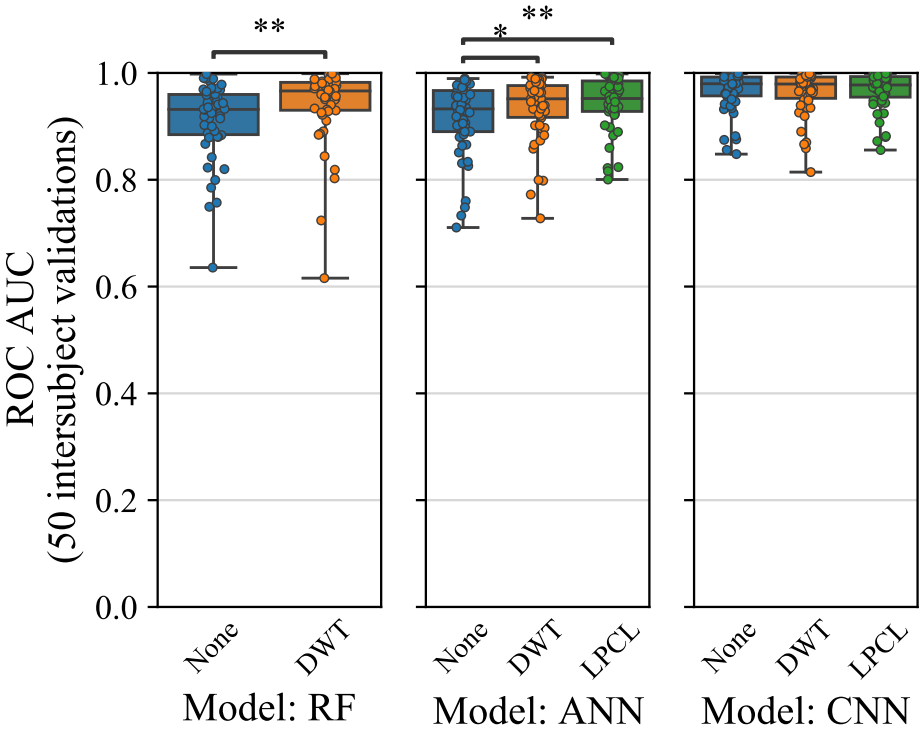

FIGURE 3.5: Visualized AUC results of 50 intersubject validations in understanding the differences between preprocessors. Statistical significance is indicated by an asterisk (*: $p < 0.05$, **: $p < 0.01$).

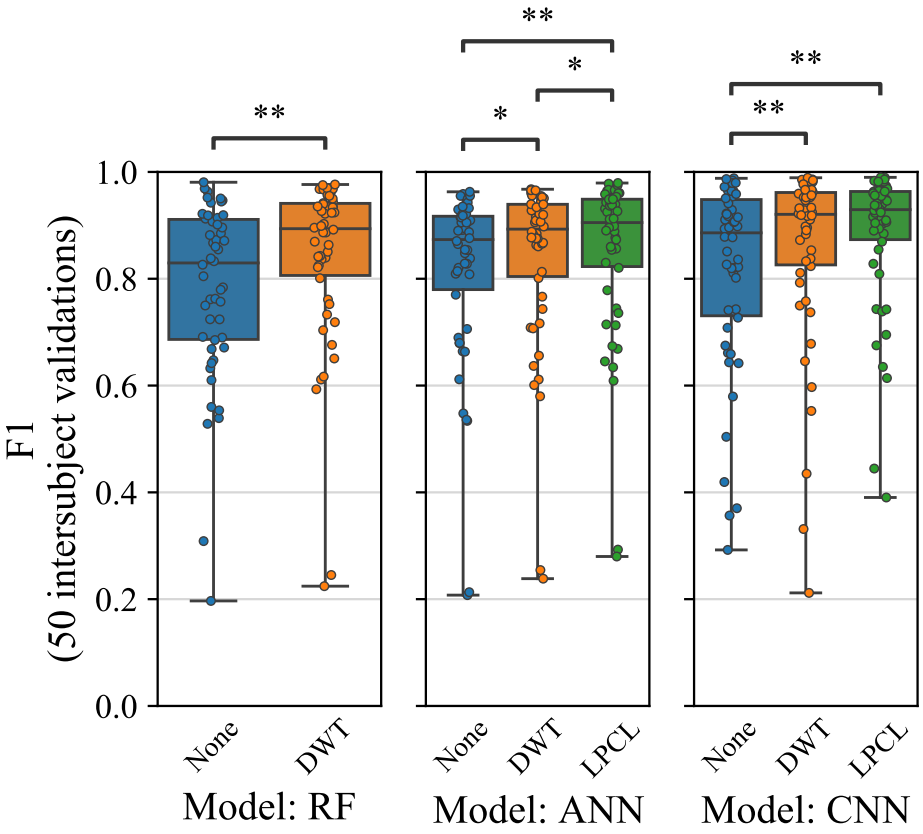

FIGURE 3.6: Visualized F1 results of 50 intersubject validations in understanding the differences between preprocessors. Statistical significance is indicated by an asterisk (*: $p < 0.05$, **: $p < 0.01$).

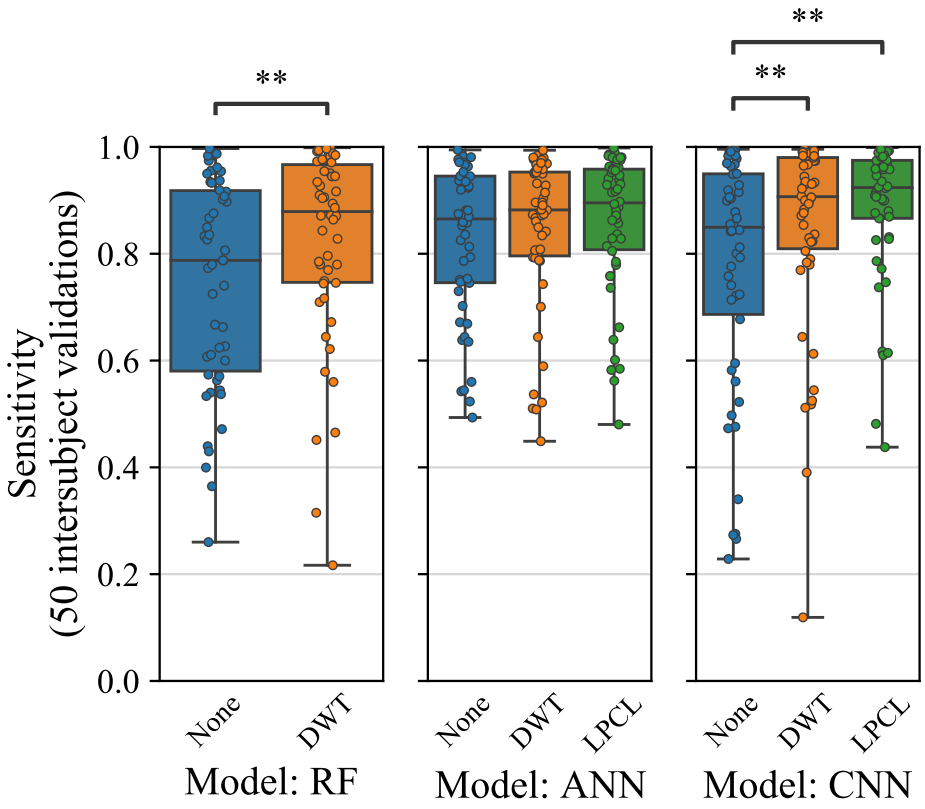

FIGURE 3.7: Visualized sensitivity results of 50 intersubject validations in understanding the differences between preprocessors. Statistical significance is indicated by an asterisk (*: $p < 0.05$, **: $p < 0.01$).

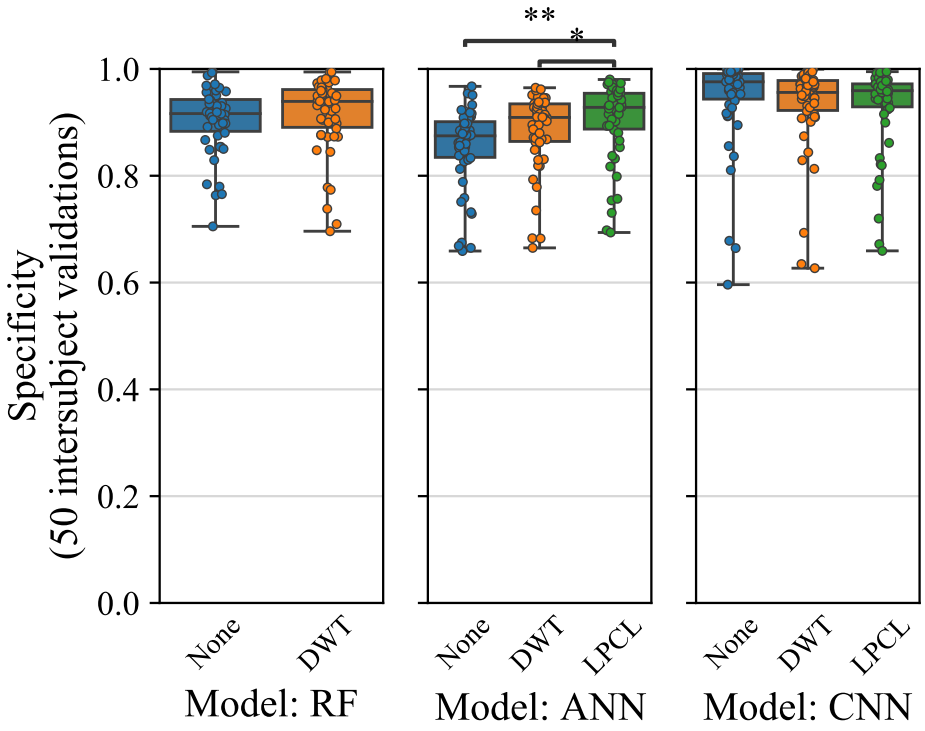

FIGURE 3.8: Visualized specificity results of 50 intersubject validations in understanding the differences between preprocessors. Statistical significance is indicated by an asterisk (*: $p < 0.05$, **: $p < 0.01$).

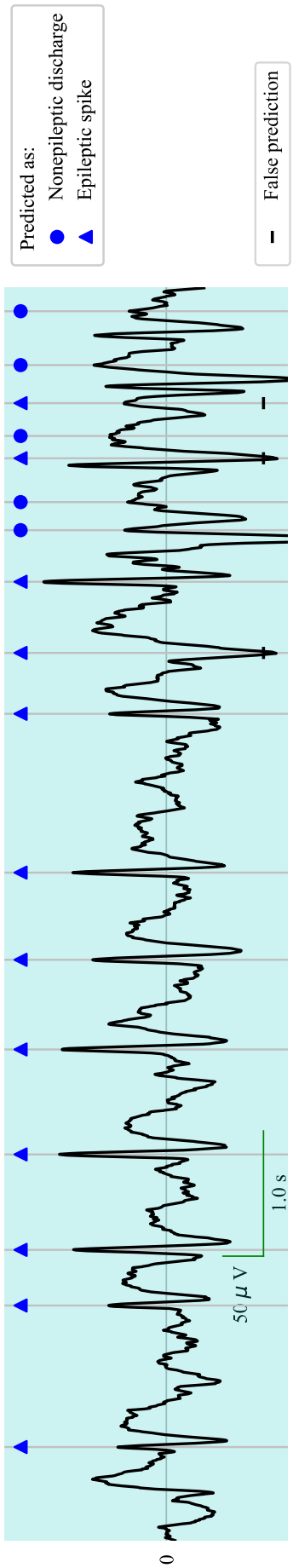

FIGURE 3.9: An example of the predicted spikes. The circles and triangles indicate nonepileptic discharges and epileptic spikes, respectively. The bars at the bottom indicate that the classification failed.

3.3 Discussion

The experimental results show that the filters with an odd symmetry constraint have a different passband, as shown in Figs. 3.10 and 3.11. This behavior is similar to a bank of filters. As Fig. 3.11(b) shows, three of the frequency bands, approximately 12, 24, and 50 Hz (the focus bands of nos. 7 and 8 are similar), are focused on by the odd symmetry LPCLs. Focusing on the adjacent peak frequencies in the spectrum, the lower frequency is approximately half of the higher frequency. Their three frequency bands can be regarded as corresponding to the standard clinical frequency bands of α, β, and γ, respectively.

In particular, the strongest response is observed in the band around 12 Hz encompassed by LPCL nos. 4 and 8, as shown in Figs. 3.10 and 3.11. Therefore, it is assumed that the features that pass through LPCLs of nos. 4 and 8 have a significant impact on the inference results. To confirm this hypothesis, we performed an additional validation to detect spikes in 50 patients' EEGs in a model with a specific LPCL disabled. In this validation, the model is trained on 49 patient EEGs as in 3. After training, to partially enable the following LPCLs, the weight coefficients of the other LPCLs are overwritten with zero:

- LPCL nos. 1 and 5 (Only LPCLs with the filter length of 8 are enabled);
- LPCL nos. 2 and 6 (Only LPCLs with the filter length of 16 are enabled);
- LPCL nos. 3 and 7 (Only LPCLs with the filter length of 32 are enabled);
- LPCL nos. 4 and 8 (Only LPCLs with the filter length of 64 are enabled).

Using these models, spikes are detected from the EEG of one test patient. Table 3.5 summarizes the results of this validation compared to the model with all LPCLs enabled. Supplementary Figs 3.12 to 3.15 visualize the AUC and F1 results in Table 3.5. As these results demonstrate, the model with LPCL nos. 4 and 8 showed the highest detection performance when partially enabling LPCLs. This result further emphasizes that the signal around 12 Hz extracted by LPCLs is effective for spike detection. However, the results of the model using IDs 4 and 8 are lower than the model using all LPCLs, it is suggested that other bands also contain important signals.

This paper's finding showed that the filters learned from the raw EEG and that the experts' labels can be decomposed into the frequency bands contributing to the inspections. That is, the data-driven filters may emulate the logic of the physician's analysis. Another advantage of the proposed work is that fine-tuning of the frequency bands is accomplished in a data-driven manner, such that the performance of the classifier is enhanced ($\mathrm{AUC} = 0.967$, $\mathrm{F1} = 0.880$), as shown in Table 3.4. Considering medical applications, the fact that the combination of LPCLs with CNN has achieved higher sensitivities than other methods [19, 35] is promising, as shown in Fig. 3.7.

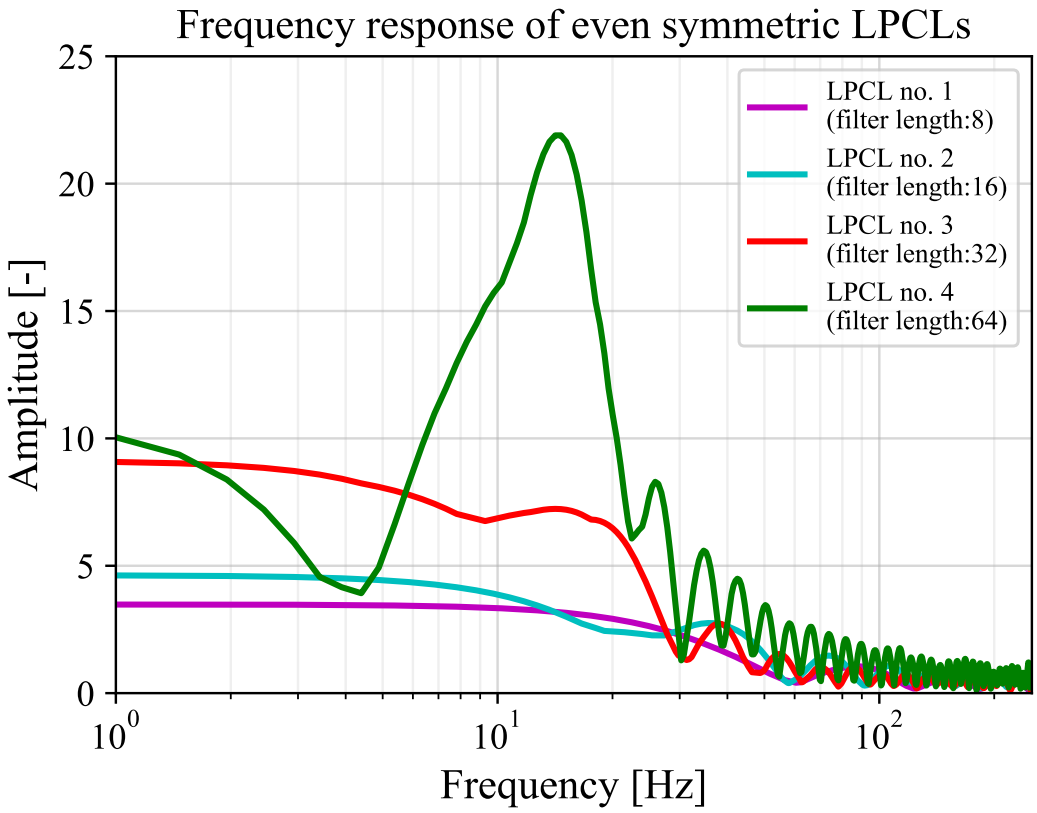

(a) Even symmetric LPCLs (LPCL nos. 1–4)

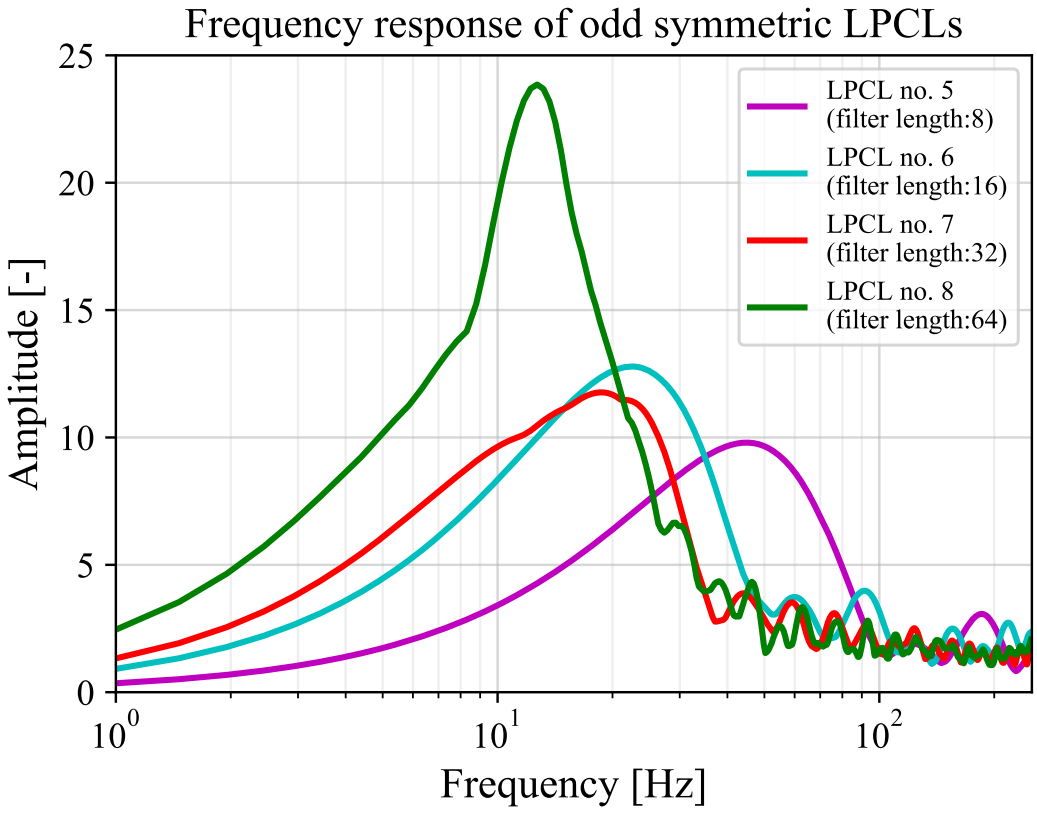

(b) Odd symmetric LPCLs (LPCL nos. 5–8)

FIGURE 3.10: An example of mean filter spectrums at the LPCL combining with ANN.

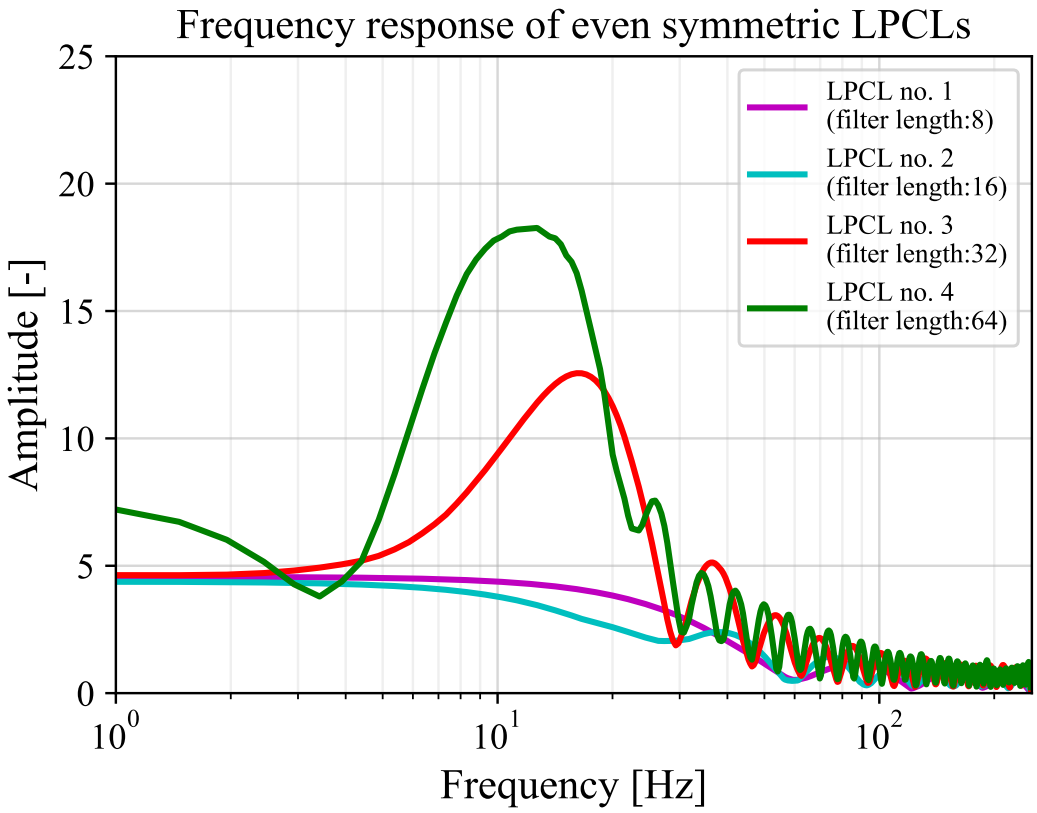

(a) Even symmetric LPCLs (LPCL nos. 1–4)

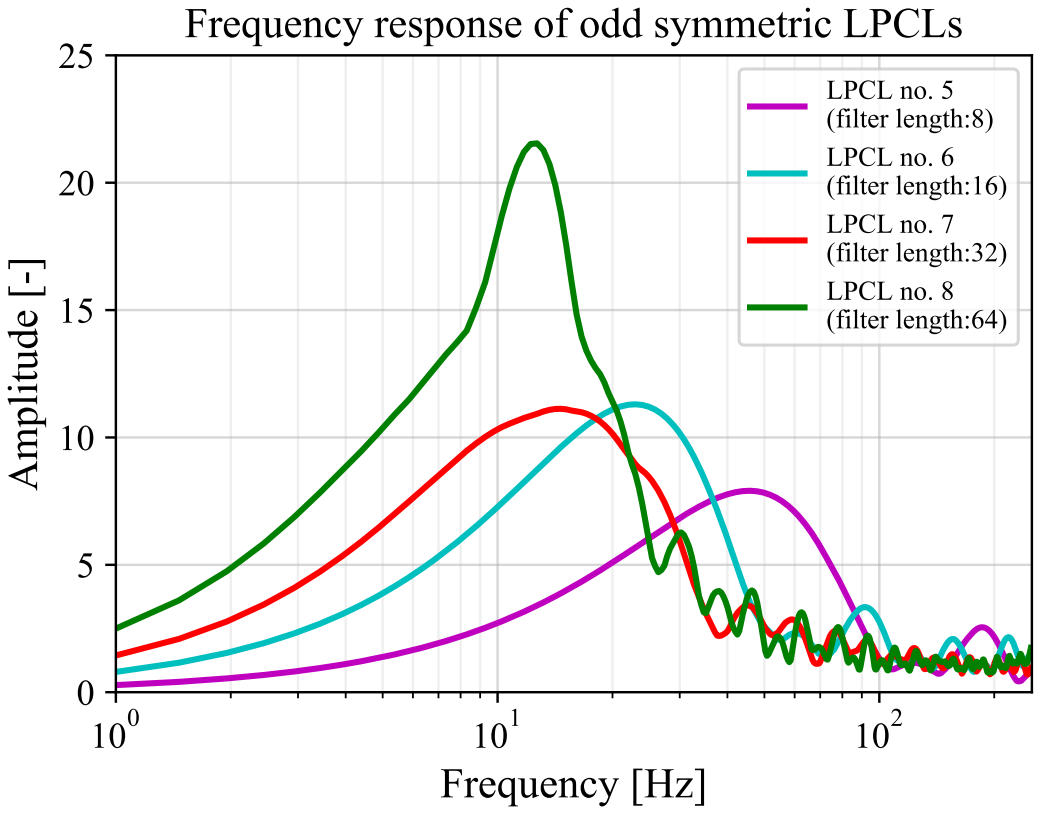

(b) Odd symmetric LPCLs (LPCL nos. 5–8)

FIGURE 3.11: An example of mean filter spectrums at the LPCL combining with CNN.

TABLE 3.5: Numerical evaluation results using the models with partial LPCL enabled. Total of 50 intersubject validations are conducted, with 30 independent runs per test patient data. Thus, a mean of 1,500 runs is calculated (Mean ± STD).

Metric	**Classification model**									
	ANN with the LPCLs					CNN with the LPCLs				
	Enabled LPCL ID									
	1, 5 (filter length: 8)	2, 6 (filter length: 16)	3, 7 (filter length: 32)	4, 8 (filter length: 64)	All	1, 5 (filter length: 8)	2, 6 (filter length: 16)	3, 7 (filter length: 32)	4, 8 (filter length: 64)	All
AUC	0.606 ± 5.69E-02	0.671 ± 6.82E-02	0.782 ± 6.99E-02	0.881 ± 7.06E-02	0.944 ± 4.99E-02	0.823 ± 7.40E-02	0.837 ± 6.64E-02	0.866 ± 6.27E-02	0.899 ± 5.85E-02	0.967 ± 3.54E-02
F1	0.044 ± 3.71E-02	0.114 ± 6.87E-02	0.357 ± 1.28E-01	0.660 ± 1.61E-01	0.850 ± 1.54E-01	0.408 ± 1.18E-01	0.466 ± 1.27E-01	0.563 ± 1.47E-01	0.697 ± 1.50E-01	0.880 ± 1.34E-01
Sensitivity	0.034 ± 3.33E-02	0.088 ± 6.21E-02	0.296 ± 1.22E-01	0.595 ± 1.65E-01	0.859 ± 1.30E-01	0.374 ± 1.16E-01	0.434 ± 1.30E-01	0.525 ± 1.42E-01	0.688 ± 1.43E-01	0.883 ± 1.31E-01
Specificity	0.988 ± 1.29E-02	0.984 ± 1.53E-02	0.968 ± 2.66E-02	0.935 ± 3.71E-02	0.904 ± 7.28E-02	0.889 ± 6.57E-02	0.887 ± 6.06E-02	0.895 ± 6.05E-02	0.868 ± 7.06E-02	0.927 ± 8.01E-02

Moreover, the LPCLs achieves these advantage points with a small computational complexity. As shown in (3.3) and (3.4), an LPCL consist of $L/2$-time additions (or subtractions) and an inner product calculation of size $L/2$. That is, only $L/2$ parameters ($h_0, h_1, \ldots, h_{\mathrm{L}/2-1}$) are increased at the inner product calculation as learning parameters. In the proposed model shown in Fig. 3.4, there are a total of eight LPCLs with four different lengths ($L = 8, 16, 32,$ and 64) and two constraint types, even and odd. In this case, the total number of parameters in the LPCLs is 120 only. Note that since the total number of parameters in the CNN-based model is approximately 3,500, the ratio of the number of parameters in the LPCLs to the all model's parameters is less than 4%. Therefore, the ratio of the LPCL parameters in the overall architecture is relatively low. However, because the proposed method is designed based on neural networks, it cannot be combined with traditional classifiers like RF. In addition, similar to standard convolutional layers, it still requires a manual setting of hyperparameters such as the kernel size and number of filters. Considering these limitations, using DWT to decompose the EEG into clinical frequency bands [19, 52, 53] would prove to be better when it comes to versatility.

Next, we investigated the characteristics of the 1-s segments to consider the effectiveness of the frequency band extracted by the LPCLs. To determine the differences of spectra between the nonepileptic discharge segments and epileptic spike segments, statistical analyses were performed on the amplitude distributions at each frequency using Welch's t-test [65]. Then, the effect sizes were calculated using Cohen's d [66]. Fig. 3.16 shows the mean spectrum of all 15,004 discharges, the mean spectrum of all 15,833 epileptic spikes, the areas where $p < 0.01$ in the t-test, and the effect sizes. Fig. 3.16 shows that there are significant differences ($p < 0.01$) in the amplitudes of almost all frequencies. In addition, in the range of 5–15 Hz, there

is a large difference ($d \approx 0.8$) between the two classes. Similarly, the LPCLs, especially no. 8, as shown in Fig. 3.10(b), showed a strong response to this significantly different low-frequency band. This resulted in LPCLs that can extract the frequency bands of statistical interest in the proposed data-driven approach. Furthermore, because the methods using the LPCL and the predefined filter of 4–64 Hz exhibit comparable performance, as shown in Fig. 4.3, a frequency band such as those shown in Figs. 3.10 and 3.11—less than 30 Hz, as roughly estimated—rather than a much higher frequency band is sufficient for epileptic spike detection.

Finally, we consider the advantage of the dataset. Table 3.6 summarizes the datasets from similar studies. It should be emphasized that the dataset constructed in this paper achieved a much larger dataset (15,833 epileptic spike waveforms from 15,004 patients) than previous studies, in which the largest dataset in terms of spike waveforms consisted of 7,500 samples [32] and the largest one in terms of patients consisted of 50 patients [67]. Note that neither of the datasets from the previous studies is publicly available. To the best of our knowledge, the number of epileptic spike segments is the largest in the literature on epileptic spike detection. This number of segments strongly supports the credibility of the statistical validation in this paper. However, more non-epileptic labels would be needed for the task of finding epileptic spikes in whole EEG recordings, rather than for the EEG segment classification task, as in this work. Moreover, the results of this paper may be limited by the fact that all patients' symptoms are CECTS.

In the design of this dataset, we set the segment's length as 1 s, following other studies [19, 45] and the annotation tasks performed by the five specialists. Of course, certain studies have used different length segments [25, 32]. As the results of this paper show, 1-s extraction is sufficient to achieve a high

TABLE 3.6: summary of the datasets on epileptic spike detection in other studies

Reference and publication year	**#Labels annotated as epileptic spikes**	**#Patients**
Wilson et al. [67], 1999	2,400	50
Indiradevi et al. [30], 2008	684	22
Liu et al. [69], 2013	142	12
Johansen et al. [32], 2016	7,500	5
Douget et al. [19], 2017	2,157	17
Xuyen et al. [25], 2018	1,491	19
Thanh et al. [26], 2020	1,442	17
This study	15,833	15,004

AUC (> 0.9 in most cases) for CECTS spikes. In particular, because epileptic spike-wave discharges in CECTS patients are known to contain a 3–4 Hz component [68], a segment length of 1 s can fully contain one of these discharges. Furthermore, even if the position of extracting the spike waveform is slightly misaligned, it is unlikely that any part of the waveform will be lost; thus, the 1-s extraction is appropriate.

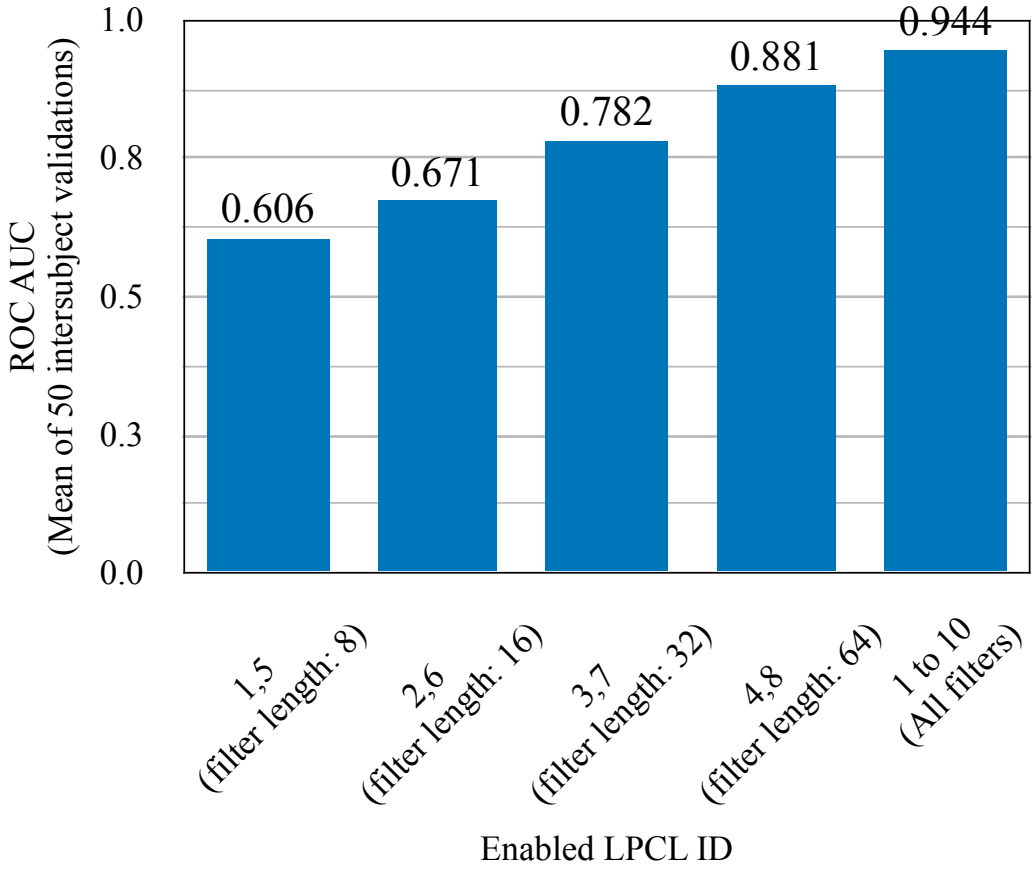

FIGURE 3.12: AUC results using ANN-based models with partial LPCL enabled.

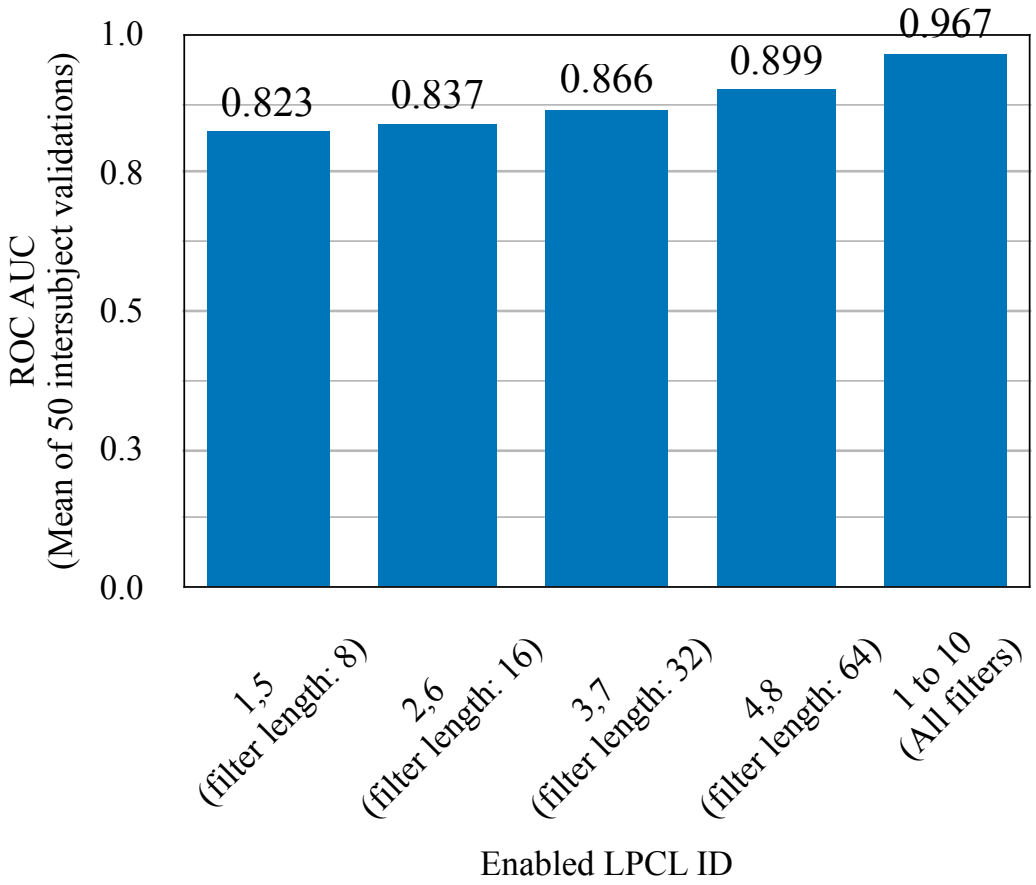

FIGURE 3.13: AUC results using CNN-based models with partial LPCL enabled.

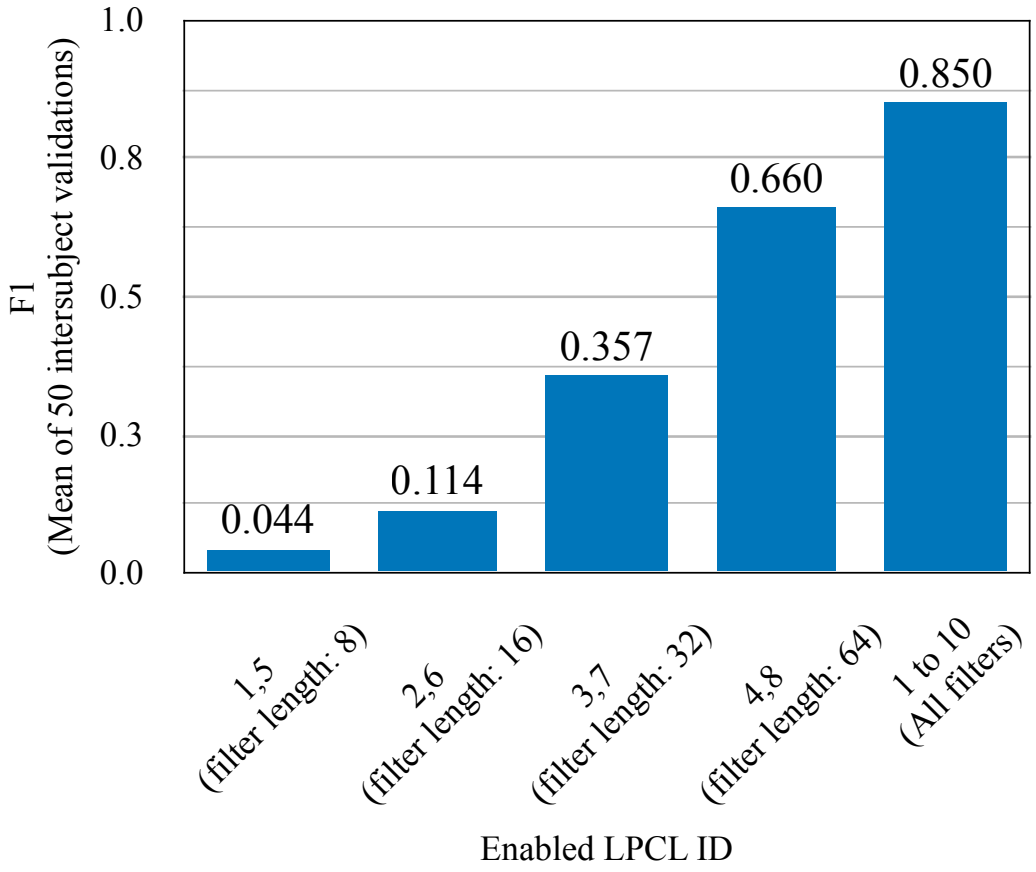

FIGURE 3.14: F1 results using ANN-based models with partial LPCL enabled.

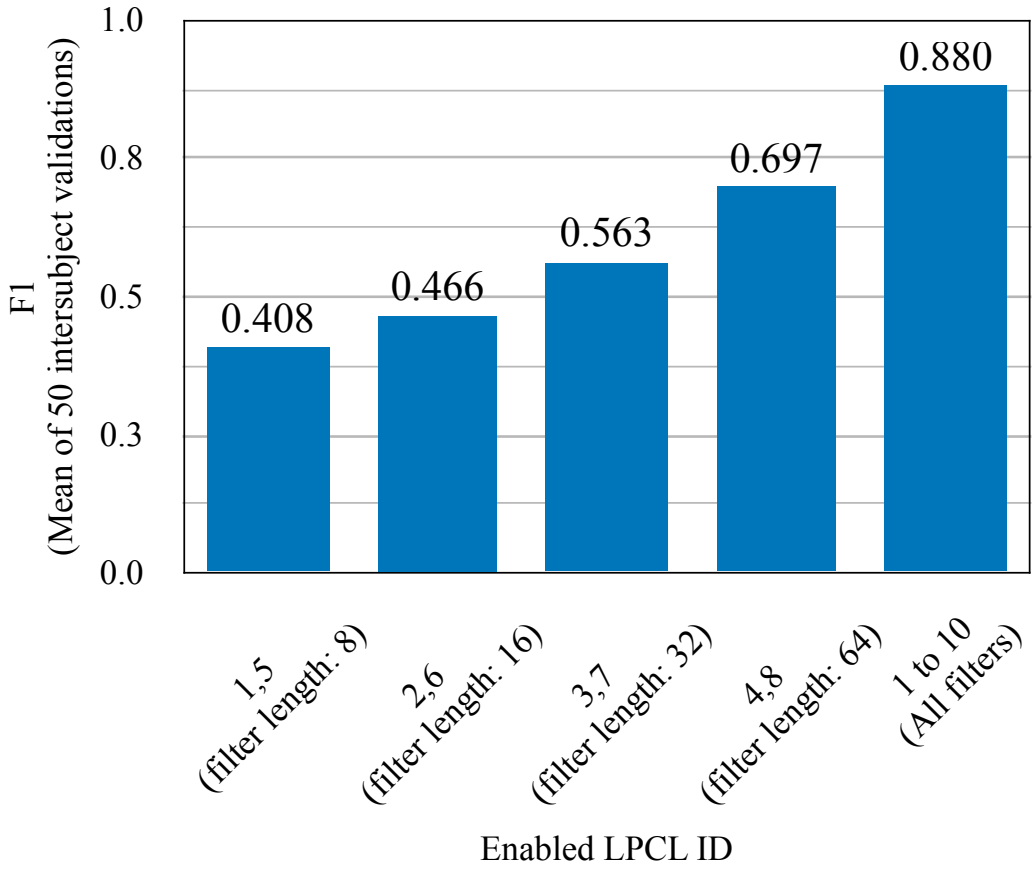

FIGURE 3.15: F1 results using CNN-based models with partial LPCL enabled.

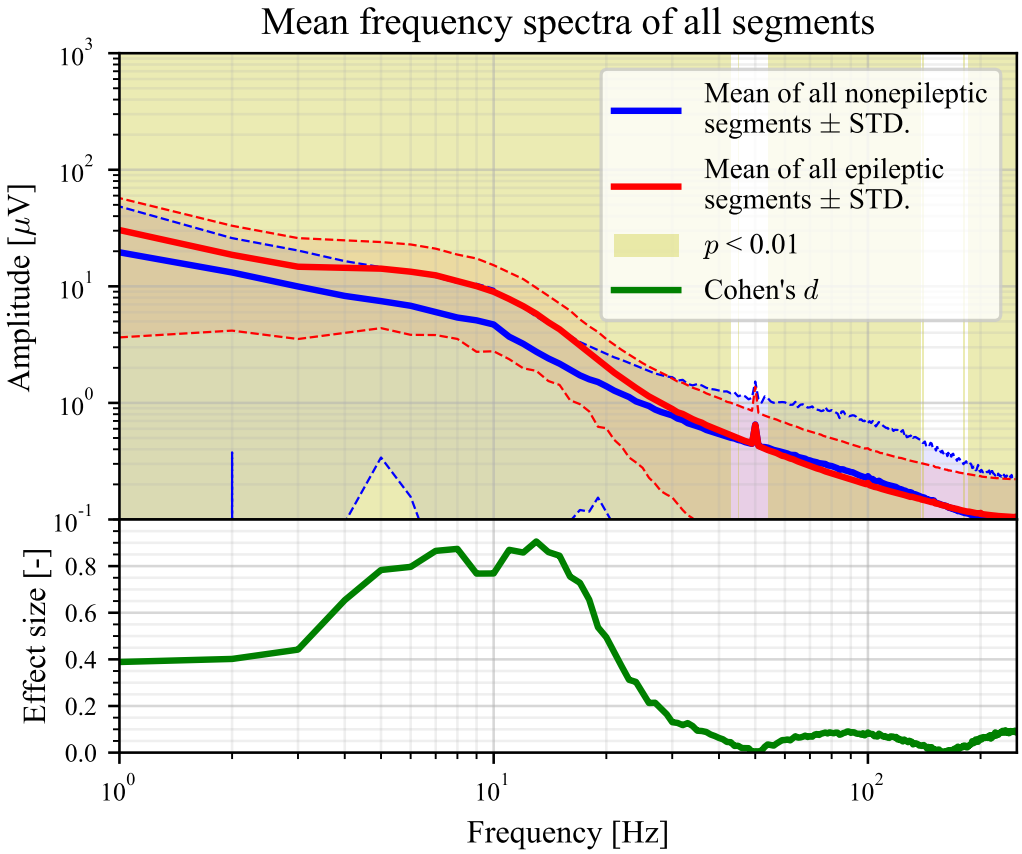

FIGURE 3.16: The mean spectrum of all 15,004 segments of nonepileptic discharges and the mean spectrum of all 15,833 segments of epileptic spikes. The areas where $p < 0.01$ in the t-test between the two classes at each frequency are filled in with yellow, and the bottom of the graph shows its effect size.

Chapter 4

Temporal Features Extraction

In this cahpter, we introduce the Satelight model, which uses the self-attention (SA) mechanism. The model was trained using a clinical EEG dataset labeled by five specialists, including 16,008 epileptic spikes and 15,478 artifacts from 50 children. The SA mechanism is expected to reduce the number of parameters and efficiently extract features from a small amount of EEG data. To validate the effectiveness, we compared various spike detection approaches with the clinical EEG data.

4.1 Proposed Method

4.1.1 Dataset Construction

Table 4.1 summarizes the dataset. Interictal EEG recordings were collected from 50 children (23 males and 27 females) with either CECTS or focal epilepsy [12] at the Department of Pediatrics, Juntendo University Nerima Hospital. The patients' ages at the time of the examination ranged between three and twelve years. The data were recorded from 16 electrodes with the International 10–20 system using the Nihon Koden EEG-1200 system. The sampling frequency was 500 Hz. This dataset was recorded and analyzed with the approval from the Juntendo University Hospital Ethics Committee and the Tokyo University of Agriculture and Technology Ethics Committee.

Measurement EEG recordings were pre-processed as follows. First, using Scipy [51], a peak search method was used to find the EEG's peak waveforms (minima and maxima)with. With a minimum distance of 100 points, this function extracts both the upward and downward peaks. Meaningless peaks caused by noise and other factors were removed using a threshold set at the 80th percentile of all peaks in one electrode. Second, for the peaks (namely, candidate spikes) that were actual epileptic spikes (spike or spike-and-wave), five experts annotated labels as epileptic. To produce accurate non-epileptic segments, the experts also labeled non-epileptic discharges. These expert-selected non-epileptic discharges, which were mistakenly detected as candidate spikes, included electromyograms, ambient noise, and alpha EEG. Finally, the EEG recordings were cropped every 1.024 s (512 sampling points) from the beginning of the recordings, independent of the temporal locations of the labeled events. As shown in Fig. 4.1, each segment that contained either epileptic or non-epileptic labeled EEG was extracted as

a valid segment. According to Fig. 4.1, segments with one or more epileptic spikes are considered epileptic segments even if they have non-epileptic labels. Thus, one segment had 16 electrodes and 512 samples (1.024 s). Z-score normalization was used with the mean value and standard deviation for each segment.

TABLE 4.1: Dataset summary of 50 epileptic EEG. Two neurosurgeons, two clinical technologists, and one pediatrician labeled this dataset. The total number of labeled samples is 31,486.

#Male patients	23
#Female patients	27
Age (Ave. $\pm$ STD.)	7.9 ± 2.0
Recording duration [min] (Ave. $\pm$ STD.)	27.5 ± 3.31
#Labeled as epileptic spikes	16,008
#Labeled as non-epileptic discharges	15,478
#Total labeled samples	31,486

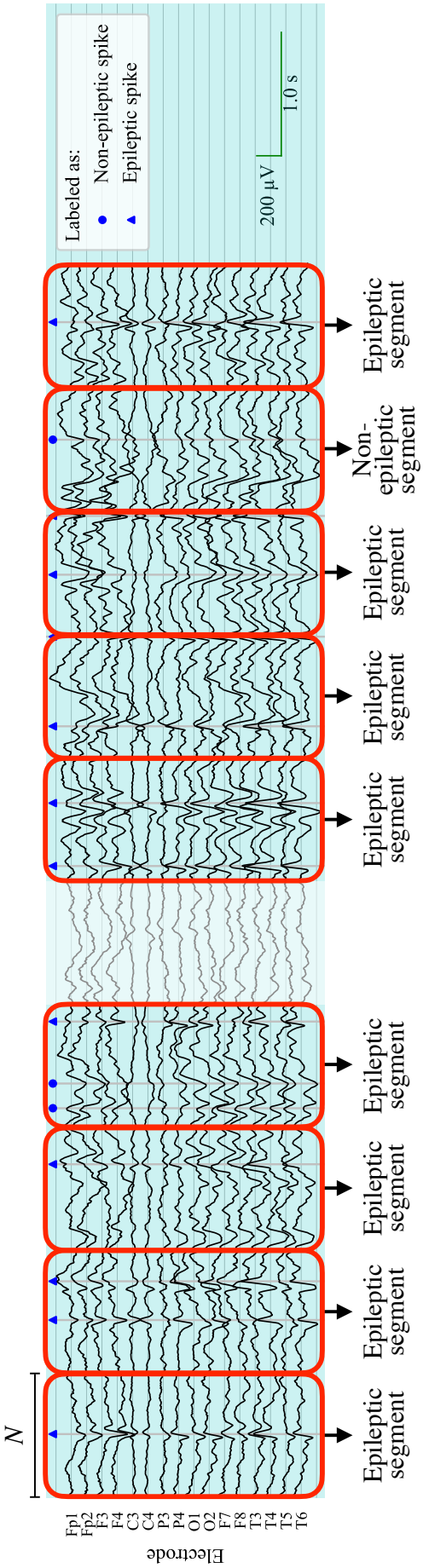

FIGURE 4.1: Example of generating segments from the EEG recordings with supervised labels. If a segment contains two distinct labels, it is deemed an epileptic segment. Unlabeled segments are discarded owing to the possibility that unlabeled EEG segments may have epileptic spikes, they are discarded. N is the length of the segment and is set to 512 (1.024 s).

4.1.2 Satelight: A self-attention-based lightweight model

In this study, we propose a model that can be trained using multi-electrode EEG segments and labels that indicate whether the spikes are epileptic. Fig. 4.2 illustrates the architecture of the proposed Satelight. As shown in Fig. 4.2, the model is factorized into the first convolution block and three SA blocks. The first convolution block combines temporal and spatial convolutions, whose effectiveness in lowering the learnable parameters has been reported in [46, 37]. A two-dimensional convolution layer with a kernel size of $(f_s/2, 1)$ implements the temporal convolution. Because the temporal kernel size is half that of the sampling frequency, it theoretically constitutes a filter with a frequency resolution of 2 Hz [46]. Spatial convolution is performed using a two-dimensional depthwise convolution layer. In this layer, 16 input matrices of size (N, C) are independently convolved with C-sized kernels. Thus, it is expected that the desired electrodes will be selected. These convolutions feed the following SA blocks with the features that have been spatiotemporally filtered. Therefore, every 8 ms, the SA layer is expected to search for relationships between feature vectors. Finally, the fully connected layer with sigmoid activation is adopted as the output layer for binary classification. For training Satelight, cross-entropy, which is the log-likelihood of the Bernoulli distribution, is employed as the loss function:

$$J = -l^{(i)} \log p^{(i)} - (1 - l^{(i)}) \log (1 - p^{(i)}), \tag{4.1}$$

where $l^{(i)} \in \{0, 1\}$ and $p^{(i)} \in [0, 1]$ denote the annotated label and the model's prediction of the i-th EEG segment, respectively.

4.1.3 Experimental implementation

To verify the effectiveness of the proposed Satelight, we conducted a numerical experiment using surface EEGs recorded from patients with epilepsy. As mentioned, this experiment is a binary classification of segments that contain or do not contain epileptic spikes. The following five NN-based models, one statistical property-based model, and one commercially available software, a non-NN-based method are used as comparison models:

- NN-based models:
  - The proposed model (Satelight);
  - Thomas et al.'s model [38];
  - Two models proposed by Jing et al. [37] with the kernel size of all temporal convolutional layers set to:
    - three (SpikeNet3);
    - five (SpikeNet5);
  - Lawhern et al.'s model (EEGNet) [46];
- Statistical property-based model:
  - Janca et al.'s model [70];
- Commercially available software:
  - Persyst13 software [40].

Note that the above NN-based model was developed to detect spikes from properly aligned EEG.

In this experiment, 50 leave-one-patient-out tests were performed using EEG segments from 49 patients as a training set and the remaining segments

from one patient as a test set in all possible combinations. The Adam optimizer [59] used the training set to train the models for comparison. Additionally, early stopping [60] was applied using a portion of the training set (namely, the validation set) to suppress overlearning. The validation set consists of 20% randomly selected segments from the training data. Thus, 80% of the segments were used for training in the 49 EEG recordings. The Xavier initializer [58] was used to generate the initial weights for this model. Note that the training process was not conducted on Persyst13 software. To compare the classification performances, we used four evaluation criteria: the AUC of the ROC, F1-value, sensitivity, and FPR.

This experiment was computed using Python 3.7.6 with Keras [62] and Scikit-learn [63] on a high-performance computer built with an AMD(R) EPYC(TM) 7742 CPU@2.25 GHz, 512 GB RAM, and four NVIDIA(R) A100 GPUs.

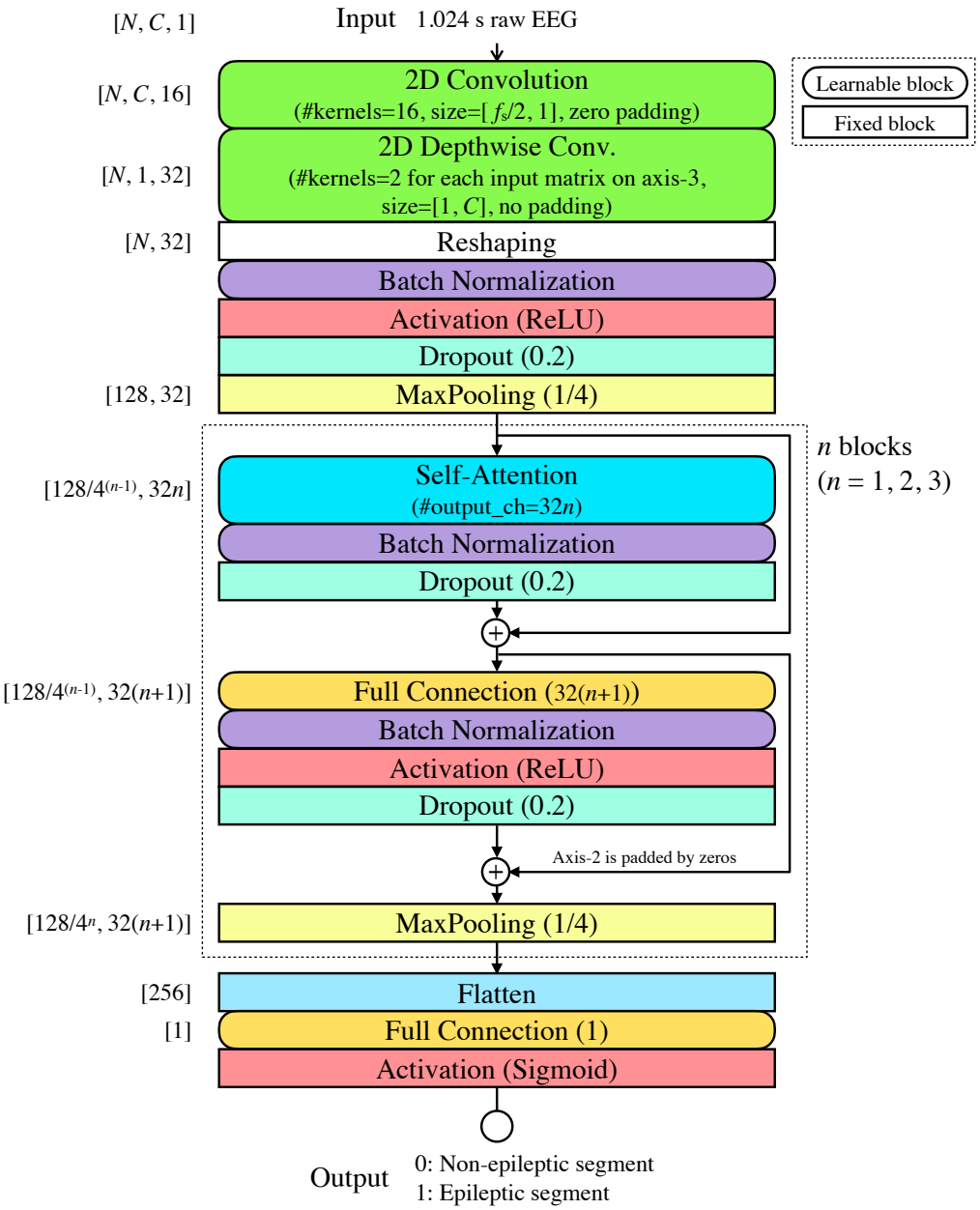

FIGURE 4.2: Architecture of the proposed Satelight, where N, C, and f_s are the length of the input segment, the number of EEG electrodes, and the sampling frequency, respectively. In this study, $N = 512$, $C = 16$, and $f_s = 500$.

4.2 Results

4.2.1 Results of spike detection performance

Table 4.2 shows the averaged numerical results of the 50 leave-one-patient-out tests. According to Table 4.2, the proposed method outperformed all evaluation metrics except AUC. Friedman's one-way analysis of variance (ANOVA) [64] showed that the effects of the models on two metrics—F1 and AUC—were significant (${\chi^2}_{\mathrm{F1}}(4) = 98.6$, $p_{\mathrm{F1}} = 1.95 \times 10^{-20}$, $W_{\mathrm{F1}} = 0.499$, ${\chi^2}_{\mathrm{AUC}}(4) = 130$, $p_{\mathrm{AUC}} = 4.93 \times 10^{-27}$, and $W_{\mathrm{AUC}} = 0.648$, where W denote Kendall's Coefficient of Concordance [64]). To better understand the effectiveness of the models, we performed a Bonferroni *post-hoc* test [64] because the main effect of the models has been observed. Fig. 4.3 presents the numerical results and the statistical analysis of the variance of 50 leave-one-patient-out tests. According to Fig. 4.3, the performance of SpikeNet and Satelight was found to be statistically different from that of EEGNet and Thomas et al.'s model. Although no statistical difference was found between SpikeNet and Satelight, SpikeNet consists of 24 convolutional layers.

TABLE 4.2: Numerical results of the 50 leave-one-patient-out tests. The best scores for each metric are in bold. Note that TPR is also known as sensitivity, one of the metrics.

Model	**Accuracy** $\pm$ STD	**F1** $\pm$ STD	**TPR** $\pm$ STD	**FPR** $\pm$ STD	**Specificity** $\pm$ STD	**AUC** $\pm$ STD
Satelight (proposed model)	$\mathbf{0.876 \pm 0.0727}$	0.843 ± 0.168	0.825 ± 0.199	$\mathbf{0.133 \pm 0.0999}$	$\mathbf{0.867 \pm 0.0999}$	0.907 ± 0.0855
EEGNet [46]	0.765 ± 0.131	0.700 ± 0.251	0.677 ± 0.282	0.197 ± 0.160	0.197 ± 0.804	0.833 ± 0.136
Thomas et al.'s model [38]	0.577 ± 0.180	0.705 ± 0.172	$\mathbf{0.995 \pm 0.0192}$	0.947 ± 0.107	0.053 ± 0.107	0.697 ± 0.157
SpikeNet3 [37]	0.857 ± 0.0882	0.818 ± 0.193	0.807 ± 0.223	$\mathbf{0.133 \pm 0.113}$	$\mathbf{0.867 \pm 0.113}$	$\mathbf{0.922 \pm 0.0770}$
SpikeNet5 [37]	0.860 ± 0.0834	0.821 ± 0.193	0.819 ± 0.218	0.147 ± 0.120	0.853 ± 0.120	0.920 ± 0.0776
Janca et al.'s model [70]	0.833 ± 0.113	0.796 ± 0.203	0.800 ± 0.241	0.172 ± 0.116	0.828 ± 0.116	0.814 ± 0.122
Persyst [40]	0.869 ± 0.0874	$\mathbf{0.866 \pm 0.142}$	0.957 ± 0.0686	0.268 ± 0.165	0.732 ± 0.165	0.904 ± 0.0737

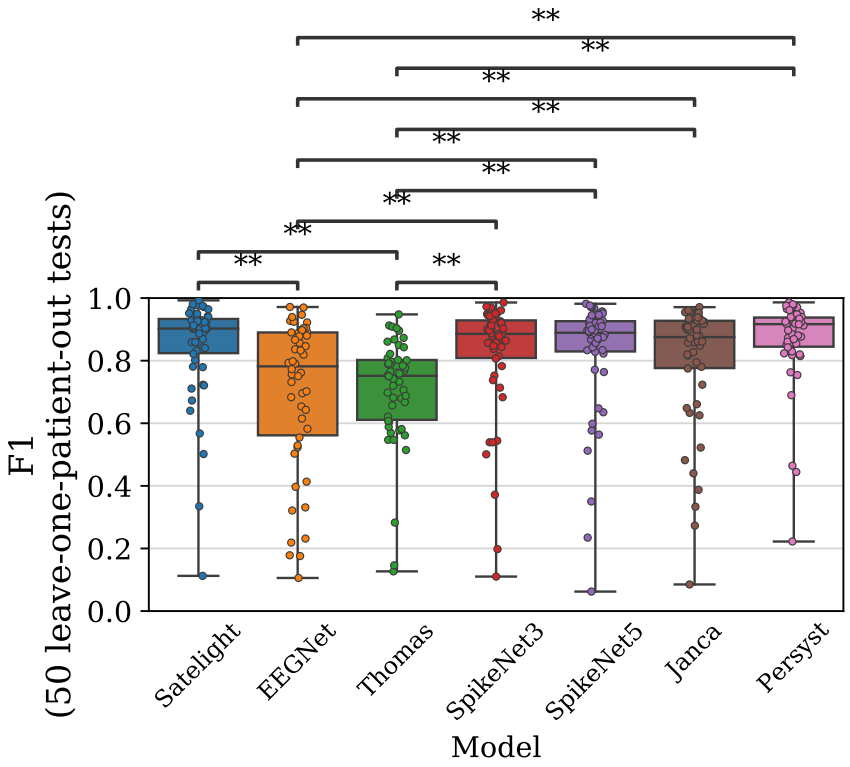

(a) F1 results of 50 leave-one-patient-out tests

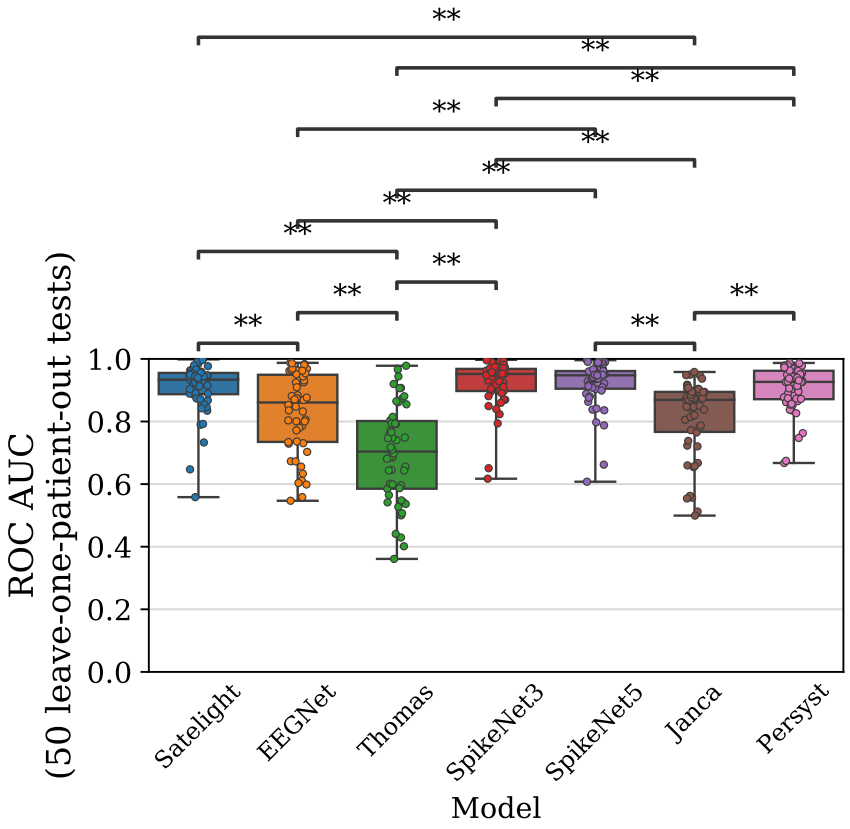

(b) AUC results of 50 leave-one-patient-out tests

FIGURE 4.3: Visualized results in understanding the differences between models. Statistical significance is indicated by an asterisk (*: $p < 0.05$, **: $p < 0.01$).

4.2.2 Results of self-attention layer behavior

In this section, we discuss an analysis of the behavior of the SA layer in Satelight. Figs. 4.4 and 4.5 show heat maps of the first SA layer's output (the size is [128, 32]), where the SA structure is illustrated in Fig. 4.2, and the upper EEG segments are input. As shown in Fig. 4.4, the epileptic spikes appeared between 0.1–0.2 s. The SA output also responded strongly in this range. Similarly, as shown in Fig. 4.5, the SA responded strongly to the epileptic spikes around 0.7 s. In this case, it did not respond to the artifacts seen around 0.3 s.

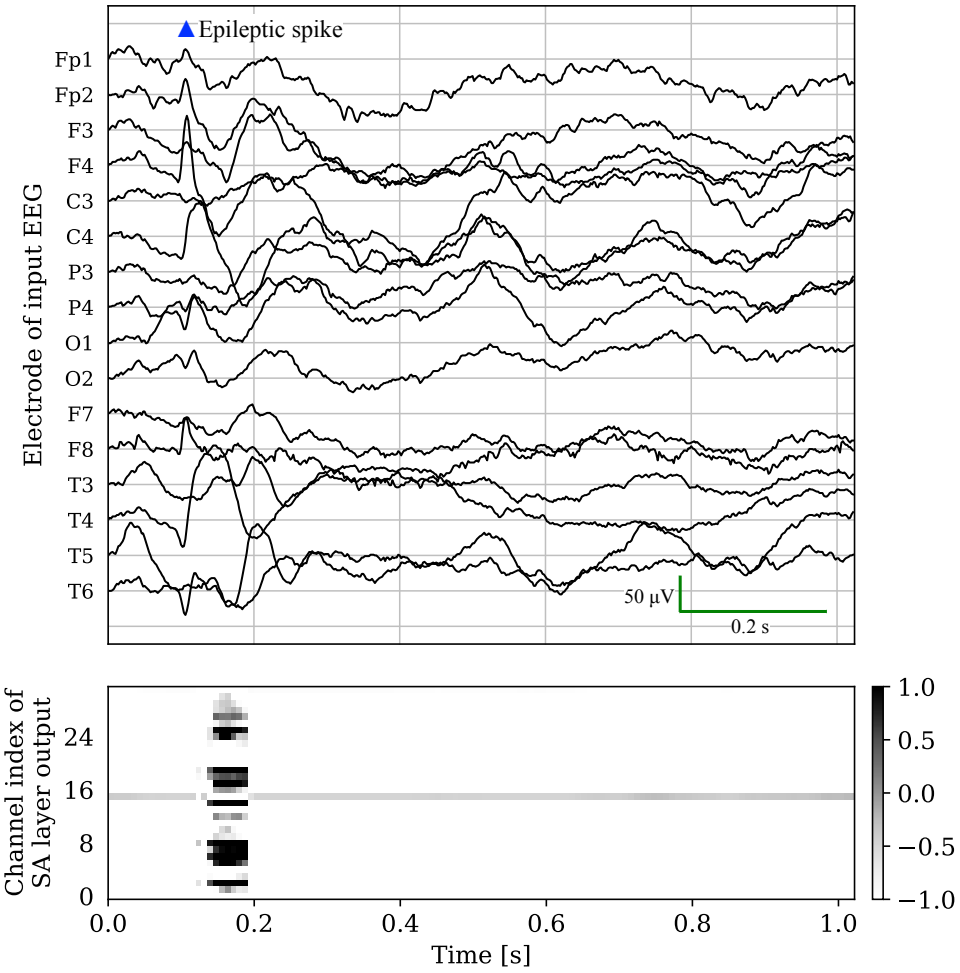

FIGURE 4.4: Example of a hidden feature map of the first SA layer (bottom) when predicting an epileptic segment (top). For better visualization, the 128 temporal points in the feature map are stretched as 1.024 s.
The peak waveform between 0.1–0.2 s is an epileptic spike.

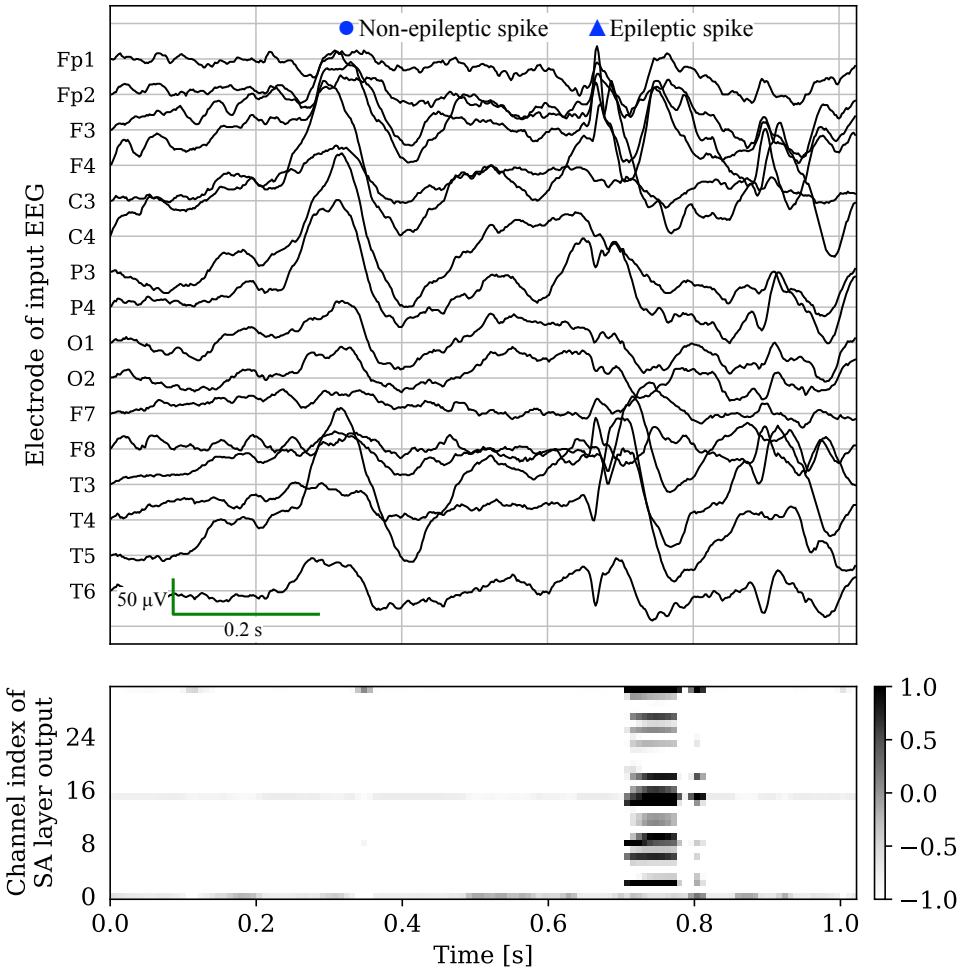

FIGURE 4.5: EExample of a hidden feature map of the first SA layer when predicting an epileptic segment with extreme artifacts at approximately 0.3 s. For better visualization, the 128 temporal points in the feature map are stretched as 1.024 s.

The peak waveform at around 0.7 s is an epileptic spike.

4.3 Discussion

4.3.1 Comparison of the number of parameters in the models

Table 4.3 and Fig. 4.6 show the number of parameters used in the numerical experiment for the compared models . EEGNet is a model with few parameters; however, as shown in Table 4.2, its detection performance is not as high as that of SpikeNet and Satelight. The model by Thomas et al., which had the highest number of parameters, produced a high FPR, as shown in Table 4.2. This might be because, although it is a deep network, it does not extract features in the spatial direction. Compared with these two models, SpikeNet is more stable in detecting epileptic spikes ($\mathrm{accuracy} = 0.860$ and $\mathrm{F1} = 0.821$ using SpikeNet5). A combination of deep convolution layers in both the spatial and temporal directions could have been achieved used to achieve this. Moreover, even though Satelight performed better at classification than SpikeNet5 ($\mathrm{accuracy} = 0.876$ and $\mathrm{F1} = 0.843$), it can be constructed with one-tenth as many parameters. This implies that the deep convolutional layer may be redundant. Therefore, using the SA layer for epileptic spike detection is effective.

4.3.2 Analysis of self-attention layer behavior

The SA layer behavior analysis results, such as the strong response during epileptic spike and no response on artifacts, as shown in Figs. 4.4 and 4.5 may imply that SA operates independently of the EEG amplitude. Moreover, these heat maps demonstrate that the SA responses are slightly delayed (≈ 200 ms) from the onset of the spike. This delay appears to be caused by specialists' focus on the positive phase reversal following the

spike [9]. According to the findings, this experiment, which classifies epileptic spikes and artifacts, does not depend on the EEG near the beginning of the event. Therefore, the behavior of the SA may change if the task involves identifying specific epileptic spike types, such as a spike–wave or sharp–wave.

4.3.3 Dataset collection

Generally, a dataset should include a variety of age, gender, and epilepsy types, as well as a large amount of data and accurate annotations. In this study, many 50 EEG recordings were collected for reliable validation. Additionally, the Z-score normalization was applied to the EEG segments to reduce amplitude differences among individuals. Therefore, we consider that the proposed model trained on this dataset has high versatility for typical epileptic spike detection.

However, the age range of the dataset was limited to children. Although it has not been reported that the typical form of epileptic spikes varies with age and gender; however, it is essential to collect patient data from a variety of age groups for reliable validation. Additionally, to build a more practical model, other epileptiforms, such as quasi-periodic spikes and poly-spike, must be annotated. To solve these limitations, it is desirable to develop a framework for more efficient data collection and labeling.

TABLE 4.3: Number of parameters of the comparison models.

Model	No. of parameters	Ratio with Satelight
Satelight (proposed model)	83,905	$\times$1.00
EEGNet [46]	3,061	$\times$0.0365
Thomas et al.'s model [38]	16,387,578	$\times$195
SpikeNet3 [37]	518,658	$\times$6.18
SpikeNet5 [37]	848,386	$\times$10.1

4.3.4 Segment extraction for dataset construction

In many spike detection studies, after detecting candidate spikes and annotating them with labels for the dataset construction, the EEG signals are segmented out based on the labeled spikes. Candidate spikes are typically found using simple signal processing methods and expert selection directly from the EEG. Single-electrode EEG studies use the former method [19, 35, 71]. The latter method is used for both single and multi-electrode EEG studies [37, 26, 38]. Because the candidate spikes are not uniquely defined, there is currently no simple segment method for multi-electrode EEG extraction. For example, detecting peak spikes based on amplitude is challenging becasue spikes do not always occur at precisely the same time over multiple electrodes. Furthermore, depending on epilepsy symptoms, the number of electrodes in which spikes appear varies; thus, the rules for candidate detection are likely to be complex.

However, if segments are extracted based on the expert's selected spikes, the validation data appear to depend on the expert's decision even, and then a data set is constructed using these segments. Therefore, for sufficient validation, the expert's decision must be removed from the factors in the validation phase. Following this justification, the dataset for this study was created using the following methodology:

1. Split the EEG recordings as segments at fixed intervals from the beginning.

2. Indicate on labels whether the segment contains epileptic spikes.

The method for extracting segments of the validation data using this procedure was superior to the method relying on expert selection. The disadvantage of this method is that the location of spikes varies for each segment;

thus, a more effective method for segment extraction or identifying characteristic waveforms for multi-electrode EEG may be necessary. In this study, the SA mechanism, as described in Section 4.2.2, rather than the segment extraction method, successfully mitigated this limitation.

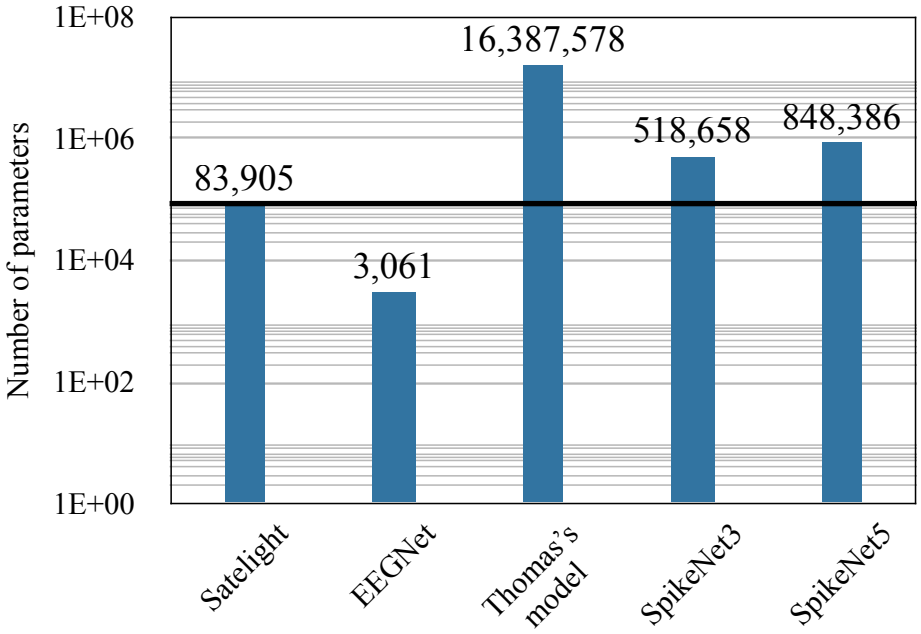

FIGURE 4.6: A visual comparison of the model parameters' numbers. The proposed model (Satelight) is lighter than the other models except for EEGNet, even though it achieves the highest accuracy of all models.

Chapter 5

Conclusion and Open Problems

5.1 Conclusion

This section presents the conclusions of the study. In this study, we have discussed the unresolved issues and challenges related to EEG-based automatic epileptic spike detection. The proposed methods

- Frequency bands extraction using for epileptic spike detection using linear-phase convolutions;
- Temporal feature extraction using self-attention-based model;

has been proposed to address the problems.

In Chapter 3, we proposed a method to combine a bank of LP filters with a NN-based model and the ability to learn its coefficients from the data. To the best of our knowledge, we have built the largest dataset in the literature, containing 30,837 samples annotated by two neurosurgeons, one clinical technologists, and one pediatrician. The proposed model classifies 1-s segments as epileptic spikes or nonepileptic discharges with high performance (AUC $>$ 0.9 in most cases). Furthermore, the filter's frequency response fitted from the EEG is strong in the low-frequency range (around 12 Hz). This band coincided brilliantly with the frequency band of interest in the raw EEG segments of epileptic spikes.

In Chapter 4, we propose a lightweight epileptic spike detection model that employs the SA mechanism. The number of parameters in this model is small compared with that of the other state-of-the-art deep NN-based models. Nevertheless, the model achieved high detection performance (accuracy $=$ 0.876 and FPR $= 0.133$). Furthermore, an exploration of the hidden parameters showed that the model automatically paid attention to the characteristic waveform locations of interest in the EEG. This would significantly contribute to the development of an explainable NN.

5.2 Open Problems

5.2.1 Limitations of collected EEG data

In all experiment of this study, the age range of the dataset was limited to children. Although it has not been reported that the typical form of epileptic spikes varies with age and gender; however, it is essential to collect patient data from a variety of age groups for reliable validation. Additionally, to build a more practical model, other epileptiforms, such as quasi-periodic spikes and poly-spike, must be annotated. To solve these limitations, it is desirable to develop a framework for more efficient data collection and labeling. It would be highly effective to use, for example, CAPTCHA [72] — using medical images instead of general photographs—to identify the system user as the specialists and simultaneously collect data annotations in the background.

5.2.2 Validity of annotation

To further improve versatility, the correctness of annotations must be examined. In this study, all samples were annotated at the sole discretion of the annotators without consulting other annotators. That is, the annotation process may contain human errors. The SpikeNet detection result in our experiment ($\mathrm{AUC} = 0.92$) was less accurate than the original result ($\mathrm{AUC} = 0.98$) reported by Jing et al. [37]. One possible reason is that only samples that six or more annotators classified as epileptic were used in their evaluation.

5.2.3 Validity of evaluation

In this study and numerous others, datasets were built using pairs of EEG segments and corresponding labels, then divided into training and test sets

for verification [19, 35, 71, 37, 26, 38]. This validation will be sufficient if spike detection can be considered a simple classification task. However, this validation method using a pre-constructed dataset is a limitation of these studies because the raw EEG recordings are not segmented. Therefore, ideally, all EEG recordings should be fully labeled by the experts without mistakes or omissions. Alternatively, detecting spikes from the entire EEG recordings and then evaluating these predictions posteriorly, rather than constructing the test set, is preferable. In other words, for practical use, a fully automated method for detecting spikes in raw EEG recordings, including EEG segmentation steps, and evaluating them appropriately is urgently required.

Appendix A

List of Publications

Journal Papers

1. **K. Fukumori**, N. Yoshida, H. Sugano, M. Nakajima, T. Tanaka, "Satelight: Self-Attention-Based Model for Epileptic Spike Detection from Multi-Electrode EEG", *Journal of Neural Engineering*, vol. 19, no. 5, pp. 055007, 2022

2. **K. Fukumori**, N. Yoshida, H. Sugano, M. Nakajima, T. Tanaka, "Epileptic Spike Detection Using Neural Networks with Linear-Phase Convolutions", *IEEE Journal of Biomedical and Health Informatics*, vol. 26, no. 3, pp. 1045–1056, 2022

3. M. S. Akter, Md. R. Islam, Y. Iimura, H. Sugano, **K. Fukumori**, D. Wang, T. Tanaka, A. Cichocki, "Multiband entropy-based feature-extraction method for automatic identification of epileptic focus based on high-frequency components in interictal iEEG," *Scientific Reports, Nature Research*, vol.10, pp.7044–7094, 2020

4. T. Wada, **K. Fukumori**, T. Tanaka, S. Fiori, "Anisotropic Gaussian kernel adaptive filtering by Lie-group dictionary learning," *PLOS ONE*, vol.15, pp.1–19, 2020

Conference Papers

1. **K. Fukumori**, N. Yoshida, H. Sugano, M. Nakajima, T. Tanaka, "Epileptic Spike Detection by Recurrent Neural Networks with Self-Attention Mechanism", *2022 IEEE International Conference on Acoustics, Speech and Signal Processing (ICASSP 2022)*, pp. 1406–1410, May 2022

2. X. Zhao, S. Takata, **K. Fukumori**, T. Tanaka, "Infant Posture Assessment Based on Rotational Keypoint Detection," *2021 IEEE Asia-Pacific Signal and Information Processing Association Annual Summit and Conference (APSIPA ASC 2021)*, SS-IVM-2.2, Online, Dec. 2021

3. Y. Miao, Y. Iimura, H. Sugano, **K. Fukumori**, T. Shoji, T. Tanaka, "Seizure Onset Zone Identification Based on Phase-Amplitude Coupling of Interictal Electrocorticogram," *2021 Annual International Conference of the IEEE Engineering in Medicine and Biology Society (EMBC 2021)*, pp.587–590, Online, Nov. 2021

4. T. Shoji, N. Yoshida, **K. Fukumori**, T. Sakai, Y. Tanaka, T. Tanaka, "SCALPNET: Detection of Spatiotemporal Abnormal Intervals in Epileptic EEG using Convolutional Neural Networks," *2020 IEEE International Conference on Acoustics, Speech and Signal Processing (ICASSP 2020)*, pp.1244–1248, Spain, May 2020

5. M. S. Akter, Md. R. Islam, **K. Fukumori**, Y. Iimura, H. Sugano, T. Tanaka, "Automatic Detection of Epileptic Focus in Ripple and Fast Ripple Bands of Interictal iEEG based on Multi-band Analysis," *2020 International Conference on Artificial Intelligence in Information and Communication (ICAIIC 2020)*, pp.490–493, Japan, Feb. 2020

6. **K. Fukumori**, T. Tanaka, "A Simple Gaussian Kernel Classifier with Automated Hyperparameter Tuning," *2019 IEEE Asia-Pacific Signal and*

Information Processing Association Annual Summit and Conference (APSIPA ASC 2019), pp.1358–1363, China, Nov. 2019

7. **K. Fukumori**, T. Nguyen, N. Yoshida, T. Tanaka, "Fully data-driven convolutional filters with deep learning models for epileptic spike detection," *2019 IEEE International Conference on Acoustics, Speech and Signal Processing (ICASSP 2019)*, pp.2772–2776, UK, May 2019

8. **K. Fukumori**, T. Tanaka "Fully data-driven optimization of Gaussian parameters for kernel classifier," *2018 IEEE Asia-Pacific Signal and Information Processing Association Annual Summit and Conference (APSIPA ASC 2018)*, pp.1858–1863, USA, Nov. 2018

9. T. Wada, **K. Fukumori**, T. Tanaka "Dictionary learning for Gaussian kernel adaptive filtering with variable kernel center and width," *2018 IEEE International Conference on Acoustics, Speech and Signal Processing (ICASSP 2018)*, pp.2766–2770, Canada, Apr. 2018

Abstracts

1. **K. Fukumori**, N. Yoshida, H. Sugano, M. Nakajima, T. Tanaka, "Epileptic Spike Detection from Multi-Channel EEG Using Self-Attention-Based Model", *2022 Annual International Conference of the IEEE Engineering in Medicine and Biology Society (EMBC 2022)*, ThEP.8, Jul. 2022

2. **K. Fukumori**, T. Tanaka, "A Simple Gaussian Kernel Classifier with Data-driven Hyperparameter Optimization," *The 5th Workshop on Electronics and Information Engineering (WEIE 2019)*, Japan, Dec. 2019

3. T. Shoji, N. Yoshida, **K. Fukumori**, T. Sakai, Y. Tanaka, T. Tanaka, "Detecting Abnormal Period in Epileptic EEG Using Deep Neural Networks," *The 5th Workshop on Electronics and Information Engineering (WEIE 2019)*, Japan, Dec. 2019

4. **K. Fukumori**, N. Yoshida, T. Tanaka, "Frequency identification for epileptic spike detection by linear-phase constrained convolutional neural network," *2019 Annual International Conference of the IEEE Engineering in Medicine and Biology Society (EMBC 2019)*, FrPOS-37.14, Germany, Jul. 2019

5. T. Shoji, N. Yoshida, **K. Fukumori**, T. Tanaka, "Detecting Abnormal Period in Epileptic EEG Using Deep Neural Networks," *2019 Annual International Conference of the IEEE Engineering in Medicine and Biology Society (EMBC 2019)*, ThPOS-35.35, Germany, Jul. 2019

6. S. Ito, **K. Fukumori**, T. Tanaka, H. Sugano, "Effective Frequency Bands and Features for Epileptic Focus Detection from Interictal Electrocorticogram," *2018 Annual International Conference of the IEEE Engineering in Medicine and Biology Society (EMBC 2018)*, ThPoS-22.25, USA, Jul. 2018

Domestic Conferences

1. **福森 航輔**, 吉田 登, 菅野 秀宣, 中島 円, 田中 聡久, "自己注意機構によるてんかん放電脳波の検出", 電子情報通信学会技術研究報告, vol.121(91), pp.11-15, ONLINE, 2021 年 7 月

2. **福森 航輔**, 吉田 登, 田中 聡久, "てんかん性脳波異常区間の検出におけるニューラルネットワークモデルの一検討", 電子情報通信学会技術研究報告, vol.119(440), pp.319–323, 沖縄, 2020 年 3 月

3. 森 滉介, **福森 航輔**, 田中 聡久, 飯村 康司, 三橋 匠, 菅野 秀宣, “EpiNet：発作間欠期頭蓋内脳波からてんかん発作起始領域を推定する畳み込みニューラルネットワーク”, 電子情報通信学会技術研究報告, vol.119(440), pp.325–330, 沖縄, 2020 年 3 月

4. **福森 航輔**, 吉田 登, 田中 聡久, “てんかん診断における脳波判読技術の評価”, 第 34 回 信号処理シンポジウム, P-19, 鳥取, 2019 年 11 月

5. 庄司 拓句, 吉田 登, **福森 航輔**, 田中 聡久, “てんかん性脳波異常区間のディープニューラルネットワークを用いた検出法”, 電子情報通信学会技術研究報告, vol.118(496), pp.217–222, 長崎, 2019 年 3 月

6. ニャムラダナー ビャムバドルジ, **福森 航輔**, 田中 聡久, 飯村 康司, 三橋 匠, 菅野 秀宣, “RNN を用いた発作間欠時脳波からのてんかん発作起始領域の推定”, 電子情報通信学会技術研究報告, vol.118(496), pp.229–231, 長崎, 2019 年 3 月

7. **福森 航輔**, 吉田 登, 田中 聡久, “ニューラルネットワークによるてんかん性スパイク検出と実効周波数帯域の同定”, 電子情報通信学会技術研究報告, vol.118(496), pp.233–235, 長崎, 2019 年 3 月

8. **福森 航輔**, 和田 智也, 田中 聡久, “カーネルロジスティック回帰におけるガウスカーネルパラメータの最適化”, 電子情報通信学会技術研究報告, vol.117(516), pp.185–190, 沖縄, 2018 年 3 月

Bibliography

[1] WHO. *Epilepsy*. www.who.int/news-room/fact-sheets/detail/epilepsy. (Accessed in June, 2021). 2021.

[2] T. J. E. Society. *Clinical Specialists Certified by JES*. square.umin.ac.jp/jes. (Accessed in March, 2021). 2021.

[3] C. Minardi, R. Minacapelli, P. Valastro, F. Vasile, S. Pitino, P. Pavone, M. Astuto, and P. Murabito. "Epilepsy in Children: From Diagnosis to Treatment with Focus on Emergency". In: *Journal of Clinical Medicine* 8.21 (2019), p. 39.

[4] B. Hermann, M. Seidenberg, and J. Jones. "The neurobehavioural comorbidities of epilepsy: can a natural history be developed". In: *The Lancet Neurology* 7.2 (2008), pp. 151–160.

[5] H. Shimizu, Y. Morimoto, N. Yamamoto, T. Tayama, and H. Ozawa. *Overlap Between Epilepsy and Neurodevelopmental Disorders: Insights from Clinical and Genetic Studies*. Exon Publications, 2022.

[6] G. Giussani, C. Franchi, P. Messina, A. Nobili, and E. Beghi. "Prevalence and incidence of epilepsy in a well-defined population of Northern Italy". In: *Epilepsia* 55.10 (2014), 1526–1533.

[7] J. Reddy and A Ramesh. "Epilepsy and Neurodevelopmental Disorders: A Biological Perspective: Epilepsy And Neurodevelopmental Disorder". In: *International Journal of Child Development and Mental Health* 7.2 (2019), pp. 55–60.

[8] A. E. Williams, J. M. Giust, W. G. Kronenberger, and D. W. Dunn. "Epilepsy and attention-deficit hyperactivity disorder: links, risks, and challenges". In: *Neuropsychiatric Disease and Treatment* 12 (2016), 287–296.

[9] M. Libenson. *Practical Approach to Electroencephalography*. Saunders, 2010.

[10] W. J. West. "On a peculiar form of infantile convulsions". In: *The Lancet* 35.911 (1841), pp. 724–725.

[11] M. Gibaud, M. Barth, J. Lefranc, K. Mention, N. Villeneuve, M. Schiff, H. Maurey, M.-A. Barthez, I. Caubel, M. Chouchane, et al. "West syndrome is an exceptional presentation of pyridoxine-and pyridoxal phosphate-dependent epilepsy: data from a French cohort and review of the literature". In: *Frontiers in Pediatrics* 9 (2021), 9:621200.

[12] W. D. Shields and O. C. Snead III. "Benign epilepsy with centrotemporal spikes". In: *Epilepsia* 50.s8 (2009), pp. 10–15. DOI: 10.1111/j.1528-1167.2009.02229.x. URL: https://onlinelibrary.wiley.com/doi/abs/10.1111/j.1528-1167.2009.02229.x.

[13] C. Varesio, M. P. Zanaboni, E. C. Salmin, C. Totaro, M. Totaro, E. Ballante, L. Pasca, P. Veggiotti, and V. De Giorgis. "Childhood Epilepsy with Centrotemporal Spikes: Clinical and Neuropsychological Outcomes 5 Years after Remission". In: *Diagnostics (Basel, Switzerland)* 10.11 (2020), p. 931. DOI: 10.3390/diagnostics10110931.

[14] R. Caplan, P. Siddarth, L. Stahl, E. Lanphier, P. Vona, S. Gurbani, S. Koh, R. Sankar, and W. D. Shields. "Childhood absence epilepsy: Behavioral, cognitive, and linguistic comorbidities". In: *Epilepsia* 49.11 (2008), pp. 1838–1846. DOI: 10.1111/j.1528-1167.2008.01680.x.

[15] L. S. Vidyaratne and K. M. Iftekharuddin. "Real-Time Epileptic Seizure Detection Using EEG". In: *IEEE Transactions on Neural Systems and Rehabilitation Engineering* 25.11 (2017), pp. 2146–2156. DOI: 10.1109/TNSRE.2017.2697920.

[16] K. E. Misulis. *Atlas of EEG, Seizure Semiology, and Management*. Oxford University Press, Oct. 2013. ISBN: 9780199985906. DOI: 10.1093/med/9780199985906.001.0001. URL: https://doi.org/10.1093/med/9780199985906.001.0001.

[17] E. Rodin, T. Constantino, S. Rampp, and P. K. Wong. "Spikes and epilepsy". In: *Clinical EEG and neuroscience* 40.4 (2009), 288–299. DOI: 10.1177/155005940904000411.

[18] M. E. Saab and J. Gotman. "A system to detect the onset of epileptic seizures in scalp EEG". In: *linical neurophysiology : official journal of the International Federation of Clinical Neurophysiology* 116.2 (2005), 427–442. DOI: 10.1016/j.clinph.2004.08.004.

[19] J. E. L. Douget, A. Fouad, M. M. Filali, J. Pyrzowski, and M. L. V. Quyen. "Surface and Intracranial EEG Spike Detection Based on Discrete Wavelet Decomposition and Random Forest Classification". In: *39th Annual International Conference of the IEEE Engineering in Medicine and Biology Society (EMBC)*. 2017, pp. 475–478.

[20] J. Gutiérrez, R. Alcántara, and V. Medina. "Analysis and localization of epileptic events using wavelet packets". In: *Medical Engineering and Physics* 23 (2001), pp. 623–631.

[21] V. Nigam and D. Graupe. "A neural-network-based detection of epilepsy". In: *Neurological Research* 26 1 (2004), pp. 55–60.

[22] I. Omerhodzic, S. Avdakovic, A. Nuhanovic, K. Dizdarevic, and K. Rotim. "Energy Distribution of EEG Signal Components by Wavelet

Transform". In: *Wavelet Transforms and Their Recent Applications in Biology and Geoscience*. Ed. by D. Baleanu. IntechOpen, 2012. Chap. 2. DOI: 10.5772/37914.

[23] Y. U. Khan, N. Rafiuddin, and O. Farooq. "Automated seizure detection in scalp EEG using multiple wavelet scales". In: *2012 IEEE International Conference on Signal Processing, Computing and Control*. 2012, pp. 1–5. DOI: 10.1109/ISPCC.2012.6224361.

[24] E. Juárez-Guerra, V. Alarcon-Aquino, and P. Gómez-Gil. "Epilepsy Seizure Detection in EEG Signals Using Wavelet Transforms and Neural Networks". In: *New Trends in Networking, Computing, E-learning, Systems Sciences, and Engineering*. Ed. by K. Elleithy and T. Sobh. Cham: Springer International Publishing, 2015, pp. 261–269.

[25] L. Xuyen, L. Thanh, D. Viet, T. Long, N. Trung., and N. Thuan. "Deep Learning for Epileptic Spike Detection". In: *VNU Journal of Science: Computer Science and Communication Engineering* 33.2 (2018). ISSN: 2588-1086. DOI: 10.25073/2588-1086/vnucsce.156. URL: http://www.jcsce.vnu.edu.vn/index.php/jcsce/article/view/156.

[26] L. T. Thanh, N. T. A. Dao, N. V. Dung, N. L. Trung, and K. Abed-Meraim. "Multi-channel EEG epileptic spike detection by a new method of tensor decomposition". In: *Journal of Neural Engineering* 17.1 (2020), p. 016023. DOI: 10.1088/1741-2552/ab5247. URL: https://doi.org/10.1088%2F1741-2552%2Fab5247.

[27] F. A. El-Samie, T. N. Alotaiby, M. Khalid, S. A. Alshebeili, and S. Aldosari. "A Review of EEG and MEG Epileptic Spike Detection Algorithms". In: *IEEE Access* 6 (2018), pp. 60673–60688. DOI: 10.1109/ACCESS.2018.2875487.

[28] C. Cheong, R. Sudirman, and S. S. Hussin. "Feature Extraction of EEG Signals Using Wavelet Transform for Autism Classification". In: *Journal of Engineering and Applied Sciences* 10.9 (2015).

[29] K. Polat and S. Günes. "Classification of epileptiform EEG using a hybrid system based on decision tree classifier and fast Fourier transform". In: *Applied Mathematics and Computation* 187 (2007), pp. 1017–1026.

[30] K. P. Indiradevi, E. Elias, P. S. Sathidevi, S. D. Nayak, and K. Radhakrishnan. "A multi-level wavelet approach for automatic detection of epileptic spikes in the electroencephalogram". In: *Computers in Biology and Medicine* 38 7 (2008), pp. 805–816.

[31] P. Fergus, D. Hignett, A. J. Hussain, D. Al-Jumeily, and K. Abdel-Aziz. "Automatic Epileptic Seizure Detection Using Scalp EEG and Advanced Artificial Intelligence Techniques". In: *BioMed Research International*. 2015.

[32] A. R. Johansen, J. Jin, T. Maszczyk, J. Dauwels, S. S. Cash, and M. B. Westover. "Epileptiform spike detection via convolutional neural networks". In: *2016 IEEE International Conference on Acoustics, Speech and Signal Processing (ICASSP)*. 2016, pp. 754–758. DOI: 10.1109/ICASSP.2016.7471776.

[33] L. Xuyen, L. Thanh, D. Viet, T. Long, N. Trung, and N. Thuan. "Deep Learning for Epileptic Spike Detection". In: *VNU Journal of Science: Comp. Science and Com. Eng* 33.2 (2017), pp. 1–13.

[34] E. Bagheri, J. Jin, J. Dauwels, S. Cash, and M. B. Westover. "A fast machine learning approach to facilitate the detection of interictal epileptiform discharges in the scalp electroencephalogram". In: *Journal of Neuroscience Methods* 326 (2019), p. 108362. ISSN: 0165-0270. DOI: https:

//doi.org/10.1016/j.jneumeth.2019.108362. URL: https://www.sciencedirect.com/science/article/pii/S0165027019302195.

[35] K. Fukumori, H. T. Thu Nguyen, N. Yoshida, and T. Tanaka. "Fully Data-driven Convolutional Filters with Deep Learning Models for Epileptic Spike Detection". In: *2019 IEEE International Conference on Acoustics, Speech and Signal Processing (ICASSP)*. 2019, pp. 2772–2776. DOI: 10.1109/ICASSP.2019.8682196.

[36] N. T. Dao, L. Thanh, N. Viet-Dung, N. Linh-Trung, and H. Le. "New Feature Selection Method for Multi-channel EEG Epileptic Spike Detection System". In: *VNU Journal of Science: Computer Science and Communication Engineering* 35.2 (2019). DOI: 10.25073/2588-1086/vnucsce.230.

[37] J. Jing, H. Sun, J. A. Kim, A. Herlopian, I. Karakis, M. Ng, J. J. Halford, D. Maus, F. Chan, M. Dolatshahi, C. Muniz, C. Chu, V. Sacca, J. Pathmanathan, W. Ge, J. Dauwels, A. Lam, A. J. Cole, S. S. Cash, and M. B. Westover. "Development of Expert-Level Automated Detection of Epileptiform Discharges During Electroencephalogram Interpretation". In: *JAMA Neurology* 77.1 (2020), pp. 103–108. ISSN: 2168-6149. DOI: 10.1001/jamaneurol.2019.3485. URL: https://doi.org/10.1001/jamaneurol.2019.3485.

[38] J Thomas, J Jin, P Thangavel, E Bagheri, R Yuvaraj, J Dauwels, R Rathakrishnan, J. J. Halford, S. Cash, and B Westover. "Automated Detection of Interictal Epileptiform Discharges from Scalp Electroencephalograms by Convolutional Neural Networks". In: *International Journal of Neural Systems* 30.11 (2020), p. 2050030. ISSN: 1793-6462. DOI: 10.1142/S0129065720500306.

[39] B. Wei, X. Zhao, L. Shi, L. Xu, T. Liu, and J. Zhang. "A deep learning framework with multi-perspective fusion for interictal epileptiform discharges detection in scalp electroencephalogram". In: *Journal of neural engineering* 18.4 (2021). ISSN: 1741-2560. DOI: 10.1088/1741-2552/ac0d60.

[40] M. L. Scheuer, A. Bagic, and S. B. Wilson. "Spike detection: Inter-reader agreement and a statistical Turing test on a large data set". In: *Clinical Neurophysiology* 128.1 (2017), pp. 243–250. ISSN: 1388-2457. DOI: https://doi.org/10.1016/j.clinph.2016.11.005. URL: https://www.sciencedirect.com/science/article/pii/S1388245716306502.

[41] C. Lourenço, M. Tjepkema-Cloostermans, and M. Putten. "Efficient use of clinical EEG data for deep learning in epilepsy". In: *Clinical Neurophysiology* 132.6 (2021), pp. 1234–1240. ISSN: 1388-2457. DOI: https://doi.org/10.1016/j.clinph.2021.01.035. URL: https://www.sciencedirect.com/science/article/pii/S1388245721004788.

[42] K. Simonyan and A. Zisserman. "Two-stream Convolutional Networks for Action Recognition in Videos". In: *Proceedings of the 27th International Conference on Neural Information Processing Systems*. Vol. 1. NIPS'14. Montreal, Canada: MIT Press, 2014, pp. 568–576. URL: http://dl.acm.org/citation.cfm?id=2968826.2968890.

[43] A. Qayyum, S. M. Anwar, M. Awais, and M. Majid. "Medical image retrieval using deep convolutional neural network". In: *Neurocomputing* 266 (2017), pp. 8–20. ISSN: 18728286. DOI: 10.1016/j.neucom.2017.05.025. URL: http://dx.doi.org/10.1016/j.neucom.2017.05.025.

[44] I. Ullah, M. Hussain, E. Qazi, and H. Aboalsamh. "An automated system for epilepsy detection using EEG brain signals based on deep learning approach". In: *Expert Systems with Applications* 107 (2018), pp. 61–71. ISSN: 0957-4174. DOI: https://doi.org/10.1016/j.eswa.2018.04.021. URL: http://www.sciencedirect.com/science/article/pii/S0957417418302513.

[45] M. Zhou, C. Tian, C. Rui, B. Wang, Y. Niu, T. Hu, H. Guo, and J. Xiang. "Epileptic seizure detection based on EEG signals and CNN". In: *Frontiers in Neuroinformatics* 12 (Dec. 2018). DOI: 10.3389/fninf.2018.00095.

[46] V. J. Lawhern, A. J. Solon, N. R. Waytowich, S. M. Gordon, C. P. Hung, and B. J. Lance. "EEGNet: a compact convolutional neural network for EEG-based brain–computer interfaces". In: *Journal of Neural Engineering* 15.5 (2018), p. 056013. DOI: 10.1088/1741-2552/aace8c.

[47] W. Huang, Y. Xue, L. Hu, and H. Liuli. "S-EEGNet: Electroencephalogram Signal Classification Based on a Separable Convolution Neural Network With Bilinear Interpolation". In: *IEEE Access* 8 (2020), pp. 131636–131646. DOI: 10.1109/ACCESS.2020.3009665.

[48] T. Shoji, N. Yoshida, and T. Tanaka. "Automated detection of abnormalities from an EEG recording of epilepsy patients with a compact convolutional neural network". In: *Biomedical Signal Processing and Control* 70 (2021), p. 103013. ISSN: 1746-8094. DOI: https://doi.org/10.1016/j.bspc.2021.103013. URL: https://www.sciencedirect.com/science/article/pii/S1746809421006108.

[49] R. M. Farsani and E. Pazouki. "A Transformer Self-Attention Model for Time Series Forecasting". In: *Journal of Electrical and Computer Engineering Innovations (JECEI)* 9.1 (2021), pp. 1–10.

[50] T. Luong, H. Pham, and C. D. Manning. "Effective Approaches to Attention-based Neural Machine Translation". In: *Proceedings of the 2015 Conference on Empirical Methods in Natural Language Processing*. Association for Computational Linguistics, 2015, pp. 1412–1421. DOI: 10.18653/v1/D15-1166.

[51] P. Virtanen, R. Gommers, T. E. Oliphant, M. Haberland, T. Reddy, D. Cournapeau, E. Burovski, P. Peterson, W. Weckesser, J. Bright, S. J. van der Walt, M. Brett, J. Wilson, K. J. Millman, N. Mayorov, A. R. J. Nelson, E. Jones, R. Kern, E. Larson, C. J. Carey, İ. Polat, Y. Feng, E. W. Moore, J. VanderPlas, D. Laxalde, J. Perktold, R. Cimrman, I. Henriksen, E. A. Quintero, C. R. Harris, A. M. Archibald, A. H. Ribeiro, F. Pedregosa, P. van Mulbregt, and SciPy 1.0 Contributors. "SciPy 1.0: Fundamental Algorithms for Scientific Computing in Python". In: *Nature Methods* 17 (2020), pp. 261–272. DOI: 10.1038/s41592-019-0686-2.

[52] J. E. Jacob, G. K. Nair, T. Iype, and A. Cherian. "Diagnosis of Encephalopathy Based on energies of EEG Subbands Using Discrete Wavelet Transform and Support Vector Machine". In: *Neurology Research International* (2018).

[53] M. M. D. Sikdar R. Roy. "Epilepsy and Seizure Characterisation by Multifractal Analysis of EEG Subbands". In: *Biomedical Signal Processing and Control* 41 (2018), pp. 264–270.

[54] E. C. Ifeachor and B. W. Jervis. *Digital Signal Processing: A Practical Approach*. 2nd. Pearson Education, 2002. ISBN: 0201596199.

[55] S. Theodoridis and K. Koutroumbas. "Chapter 6 - Feature Generation I: Data Transformation and Dimensionality Reduction". In: *Pattern*

Recognition (Fourth Edition). Ed. by S. Theodoridis and K. Koutroumbas. Fourth Edition. Boston: Academic Press, 2009, pp. 323–409. ISBN: 978-1-59749-272-0. DOI: https://doi.org/10.1016/B978-1-59749-272-0.50008-6. URL: https://www.sciencedirect.com/science/article/pii/B9781597492720500086.

[56] T. Tran, R. de Queiroz, and T. Nguyen. "Linear-phase perfect reconstruction filter bank: lattice structure, design, and application in image coding". In: *IEEE Transactions on Signal Processing* 48.1 (2000), pp. 133–147. DOI: 10.1109/78.815484.

[57] K. He, X. Zhang, S. Ren, and J. Sun. "Delving Deep into Rectifiers: Surpassing Human-Level Performance on ImageNet Classification". In: *Proceedings of the 2015 IEEE International Conference on Computer Vision (ICCV)*. ICCV '15. Washington, DC, USA: IEEE Computer Society, 2015, pp. 1026–1034. ISBN: 978-1-4673-8391-2. DOI: 10.1109/ICCV.2015.123. URL: http://dx.doi.org/10.1109/ICCV.2015.123.

[58] X. Glorot and Y. Bengio. "Understanding the difficulty of training deep feedforward neural networks". In: *Proceedings of the Thirteenth International Conference on Artificial Intelligence and Statistics*. 2010, pp. 249–256.

[59] M. Bernico. *Deep Learning Quick Reference : Useful hacks for training and optimizing deep neural networks with TensorFlow and Keras*. Packt Publishing Limited, 2018.

[60] D. Sarkar, R. Bali, and T. Ghosh. *Hands-On Transfer Learning with Python*. Packt Publishing Limited, 2018.

[61] T. Sakai, T. Shoji, N. Yoshida, K. Fukumori, Y. Tanaka, and T. Tanaka. "Scalpnet: Detection of Spatiotemporal Abnormal Intervals in Epileptic EEG Using Convolutional Neural Networks". In: *ICASSP 2020 - 2020 IEEE International Conference on Acoustics, Speech and Signal Processing (ICASSP)*. 2020, pp. 1244–1248. DOI: 10.1109/ICASSP40776.2020.9054705.

[62] F. Chollet et al. *Keras*. https://keras.io. 2015.

[63] F. Pedregosa, G. Varoquaux, A. Gramfort, V. Michel, B. Thirion, O. Grisel, M. Blondel, P. Prettenhofer, R. Weiss, V. Dubourg, J. Vanderplas, A. Passos, D. Cournapeau, M. Brucher, M. Perrot, and E. Duchesnay. "Scikit-learn: Machine Learning in Python". In: *Journal of Machine Learning Research* 12 (2011), pp. 2825–2830.

[64] S. Siegel and N. Castellan. *Nonparametric Statistics for the Behavioral Sciences*. Second. McGraw–Hill, Inc., 1988.

[65] G. D. Ruxton. "The unequal variance t-test is an underused alternative to Student's t-test and the Mann–Whitney U test". In: *Behavioral Ecology* 17.4 (May 2006), pp. 688–690. ISSN: 1045-2249. DOI: 10.1093/beheco/ark016. eprint: https://academic.oup.com/beheco/article-pdf/17/4/688/17275561/ark016.pdf. URL: https://doi.org/10.1093/beheco/ark016.

[66] J Cohen. *Statistical Power Analysis for the Behavioral Sciences*. Second. Routledge, 1988. DOI: 10.4324/9780203771587.

[67] S. B. Wilson, C. A. Turner, R. G. Emerson, and M. L. Scheuer. "Spike detection II: automatic, perception-based detection and clustering". In: *Clinical Neurophysiology* 110.3 (1999), pp. 404–411. ISSN: 1388-2457. URL: https://doi.org/10.1016/s1388-2457(98)00023-6.

[68] J. S. Hahn. "Neonatal and Pediatric Electroencephalography". In: *Aminoff's Electrodiagnosis in Clinical Neurology (Sixth Edition)*. Ed. by M. J. Aminoff. Sixth. London: W.B. Saunders, 2012, pp. 85–128. ISBN: 978-1-4557-0308-1. DOI: https://doi.org/10.1016/B978-1-4557-0308-1.00004-2. URL: http://www.sciencedirect.com/science/article/pii/B9781455703081000042.

[69] Y. C. Liu, C. C. K. Lin, J. J. Tsai, and Y. N. Sun. "Model-based spike detection of epileptic EEG data". In: *Sensors* 13.9 (2013), pp. 12536–12547. ISSN: 1424-3210. DOI: 10.3390/s130912536.

[70] R. Janca, P. Jezdik, R. Cmejla, M. Tomášek, G. Worrell, M. Stead, J. Wagenaar, J. Jefferys, P. Krsek, V. Komarek, P. Jiruska, and P. Marusic. "Detection of Interictal Epileptiform Discharges Using Signal Envelope Distribution Modelling: Application to Epileptic and Non-Epileptic Intracranial Recordings". In: *Brain topography* 28 (2014). DOI: 10.1007/s10548-014-0379-1.

[71] K. Fukumori, N. Yoshida, H. Sugano, M. Nakajima, and T. Tanaka. "Epileptic Spike Detection Using Neural Networks With Linear-Phase Convolutions". In: *IEEE Journal of Biomedical and Health Informatics* 26.3 (2022), pp. 1045–1056. DOI: 10.1109/JBHI.2021.3102247.

[72] L. von Ahn, M. Blum, N. J. Hopper, and J. Langford. "CAPTCHA: Using Hard AI Problems for Security". In: *Advances in Cryptology — EUROCRYPT 2003*. Ed. by E. Biham. Berlin, Heidelberg: Springer Berlin Heidelberg, 2003, pp. 294–311. ISBN: 978-3-540-39200-2.